ACCESSIBILITY
Open

OSLO METROPOLITAN UNIVERSITY
STORBYUNIVERSITETET

Master's Degree in
Structural Engineering and Building Technology
Department of Civil Engineering and Energy Technology

MASTER THESIS

THESIS TITLE	DATE
Analysis of structural effects due to ice formation inside hollow steel foundations	12.06.2020
	NUMBER OF PAGES 98
AUTHOR(S) Robert Ailenei	SUPERVISOR(S) Vagelis Plevris

IN COLLABORATION WITH	CONTACT PERSON
Statnett SF	Øyvind Welgaard

SUMMARY
This master thesis is written on behalf of Statnett SF, which is the system operator of the Norwegian power system. Statnett has developed a new type of foundation which requires less time to assemble and is more convenient to transport than a typical concrete foundation. The foundation consists of a tubular section mounted on top of a steel pad. In soils with high water content, water fills the tubular section and freezes inside when the temperature drops below 0 (°C). The thesis investigates if the water that freezes inside the tubular section of the foundation has a damaging effect. The theory of heat transfer, the behavior and the properties of ice were studied. Based on the theory, a set of analyses and calculations were conducted. The analysis revealed the amount of water that can freeze inside the tubular section and the strength capacity of the section. The conclusion based on the research and the analysis results indicates that the force exerted by ice is within the strength capacity of the foundation.

3 KEYWORDS
Steel foundation
Frost depth
Resistance to ice formation

Acknowledgements

This thesis was carried out at Statnett SF, which is the system operator of the Norwegian power system. I want to extend my thanks to the people responsible for giving me this opportunity. I would also like to thank Andreas Istad Lem from Statnett for helping when I was stuck and giving much-needed advice. Lastly, I would like to thank my supervisor, Vagelis Plevris, from Oslo Metropolitan University, for guidance and discussions during the work with this thesis.

Oslo Metropolitan University

Oslo, June 2020

Robert Ailenei

Robert Ailenei

Abstract

This master thesis is written on behalf of Statnett SF, which is the system operator of the Norwegian power system. Statnett, among other things, builds and maintains the overhead power lines. The power lines are usually supported by steel lattice towers. Further, the towers are mounted on concrete foundations. Transporting concrete foundations to remote sites, especially in the winter period, can be very costly and challenging to maintain the quality of the concrete. For this reason, Statnett has developed a new type of foundation referred to as a tubular steel foundation, which requires less time to assemble and is more convenient to transport than a typical concrete foundation.

The foundation consists of a tubular section mounted on top of a steel pad. In soils with high water content, it is assumed that water fills the tubular section and freezes inside when the temperature drops below 0 (°C). The thesis investigates if the water that freezes inside the tubular section of the foundation has a damaging effect. The theory of heat transfer, the behavior and the properties of ice were studied. Based on the theory, a set of analyses and calculations were conducted. The thermal analysis revealed the amount of water that can freeze inside the tubular section. Based on the results, three scenarios were considered critical and were further studied.

Scenario 1: Formation of an ice plug inside the tubular section
Scenario 2: Thermal expansion of the ice plug
Scenario 3: Formation of two ice plugs with water confined between them

Each scenario was further investigated from a structural perspective. Because of the foundation's geometry, the first scenario was found not to be dangerous for the foundation. For the second scenario, a model was created in the finite element analysis software Abaqus CAE to investigate the pressure resulting from the thermal expansion of ice. In the third scenario, the strength capacity of the pipe was calculated with respect to the formation of two ice plugs by hand calculations and simulation in Abaqus CAE.

The conclusion based on the research and the analysis results indicates that the force exerted by ice is within the strength capacity of the foundation.

Keywords – Steel foundation, Frost depth, Resistance to ice formation

Contents

List of Figures

List of Tables

1 Introduction

Statnett SF is a public enterprise owned by the Norwegian State and has three main goals:

- Securing a stable supply of electricity
- Facilitating the realization of Norway's climate targets
- Paving the way for value creation, for society and customers alike

Securing a stable supply of electricity requires not only the maintenance of the existing transmissions lines but also the building of new ones. A typical transmission line consists mainly of the overhead power line, lattice towers, and foundations for the towers. One of the new transmission lines that are under construction is called Balsfjord - Skaidi. The Balsfjord - Skaidi transmission line is approximately 300 km long and runs through some of the most remote parts of Northern Norway. The transmission line consists of traditional, steel, lattice towers supported by buried foundations at each of the four legs. The buried foundations are mainly of two types, concrete and steel foundations. A typical lattice tower and the concrete foundations are shown in figure 1.1.

Figure 1.1: Typical transmission tower

The foundations may be subjected to compressive forces, uplift and shear forces, or a combination of those. The concrete foundations are made on-site from concrete poured into temporary forms. In general, the concrete is transported by a helicopter to the site. In winter, the freezing temperatures in some areas present a challenge for the safe transport of concrete. Mainly, for this reason, Statnett has developed a new type of foundation made of steel. Compared to the traditional mass concrete foundations, the steel foundations are a more efficient and transport friendly solutions. The steel foundation, which is the subject of this thesis, consists of a hollow steel section connected to a steel plate, figure 1.2.

Figure 1.2: Steel foundation

The entire foundation will be buried, relying on the deadweight of the overburden soil to provide the necessary uplift resistance. The foundation buried depth is approximately three meters below ground level. The vertical hollow section that can be seen in figure 1.2 is open at the bottom, which means that in soils with high groundwater level, water enters freely inside. An uncertainty has been raised regarding the impact water has when it freezes in the hollow steel section of the foundation. The focus of this thesis is to investigate the effect freezing water has on the foundation.

1.1 Aim and objective

Some of the steel foundations on which the transmission towers are mounted may be situated in terrain with high groundwater levels, such as marsh areas. The steel foundations are primary intended for use, in the North of Norway, including the furthest - up to 70 degrees north. Up north temperatures can reach far below zero degrees Celsius, thus freezing of the groundwater is expected. As frost bursting of pipes is not uncommon, Statnett has considered this a risk that needs to be evaluated more carefully. This thesis aims to investigate the potential for the tubular section of the foundation to be damaged as a result of the water freezing.
The main objectives of the thesis are summarized below:

- Perform a set of thermal analysis to evaluate the amount of water that can freeze inside the hollow steel section of the steel foundation
- Based on thermal analysis assess if the amount of frozen water is damaging for the foundation

1.2 Scope and limitations

The scope of the thesis is confined to evaluate the effect groundwater has when it enters and freezes inside the tubular section of the steel foundation. The soil around the foundation is also taken into consideration and modeled accordingly. However, the forces created by the heaving of soil when it freezes is not in the scope of this thesis.

1.3 Thesis layout

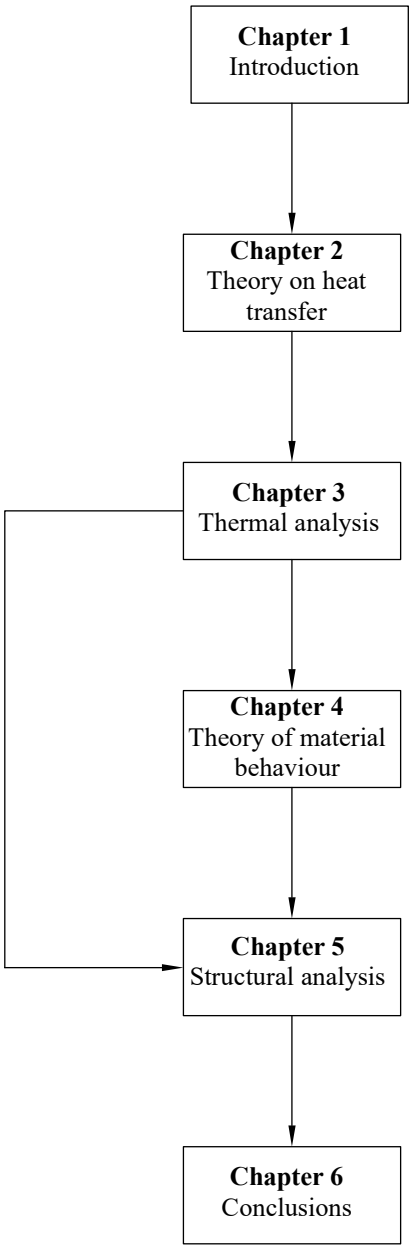

Figure 1.3: Thesis layout

Chapter 1 gives an overview of this thesis work. Chapter 2 studies the theory of the heat transfer mechanism. In chapter 3, the first two simulations are presented, which set the basis for the thermal analysis of the steel foundation. Further, chapter 4 studies the behavior of ice. With the results from chapter 3 and the theory studied in chapter 4, the foundation's structural behavior is analyzed. Chapter 6 gives the final conclusions of this thesis work.

2 Theory on heat transfer

In this chapter, the theory behind the mechanism of heat transfer in a hollow steel foundation and the propagation of temperature throughout soil and water are described. The chapter serves as a foundation for the thermal simulations, which are dealt with in a later chapter.

2.1 Heat transfer

A problem classified as being in a steady-state implies no change in temperature with time at any point within the structure. Simply put, the temperature is not dependent on time. A structure or a system in which temperature varies with time falls in the transient heat transfer category. The figure 2.1 and 2.2 show the difference between the two states described above. The steel foundation analyzed in this thesis is subjected to transient heat transfer.

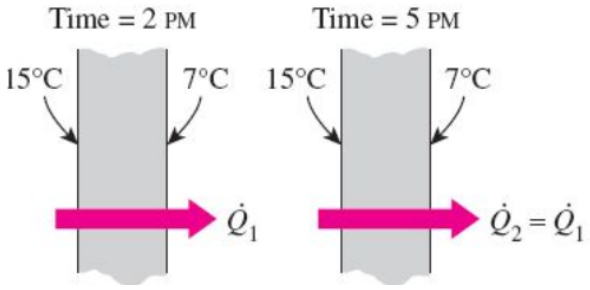

Figure 2.1: Steady state heat transfer (Cengel, 2014)

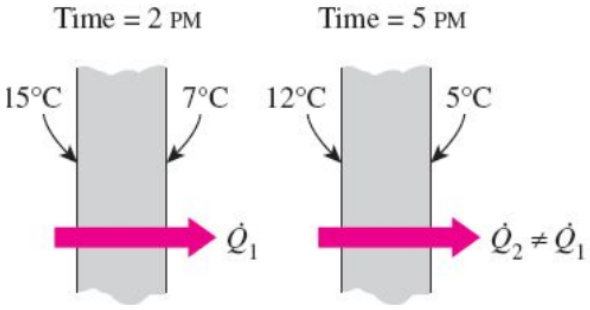

Figure 2.2: Transient state heat transfer (Cengel, 2014)

Steady-state heat transfer is illustrated in figure 2.1. Heat is transferred from the surface with a higher temperature to the surface with a lower temperature, as shown. As can be

seen, there is no change in temperature with time.
While in figure 2.2, the temperature changes over time, notice the temperature difference at 2 PM and, later, at 5 PM. Transient heat transfer implies variation with time.
Further heat transfer mechanisms are classified into three types: conduction, convection, and radiation. All three transfer methods are based on a temperature difference, and in all methods, the heat moves from the a high-temperature system to a low-temperature system.
The heat movement in the case of the steel foundation is only due to conduction and convection. Below a detailed study of the processes of conduction and convection is presented.

2.2 Internal energy and energy transfer

Before moving to the phenomena of heat transfer through conduction and convection, a study of the internal energy and energy transfer is necessary to better understand those processes. The total energy of a system is denoted E, and the internal energy is U.
The sum of all microscopic forms of energy of a system is called the internal energy. The internal energy can also be defined as the sum of the kinetic and the potential energy of the molecules in a system. By adding sufficient energy to a solid or a liquid material, the interconnecting molecular bindings will be broken, and the material can be turned into a gas. The internal energy associated with this phase change is called latent heat or latent energy.
When it comes to fluids, the internal energy of a stationary fluid is denoted u while the energy for a flowing fluid is given as (Cengel, 2014):

$$h = u + Pv \tag{2.1}$$

Where h is the enthalpy, u is the internal energy, P is pressure, and v is the volume of the system.
For gasses, the change in internal energy and enthalpy can be expressed by introducing the notion of specific heat. Specific heat is the amount of heat per unit mass required to raise the temperature by one degree Celsius. The following formulas give the change in

internal energy and the change in enthalpy (Cengel, 2014):

$$\Delta U = mc_{v,avg}\Delta T \tag{2.2}$$

$$\Delta H = mc_{p,avg}\Delta T \tag{2.3}$$

The change in internal energy is dependent on the specific heat at a constant volume donated c_v, while the enthalpy is dependent on the specific heat held at constant pressure c_p. In addition, both the enthalpy and the internal energy are dependent on the mass and the temperature of the system.
Unlike gasses, the specific heat for incompressible liquids and solids is constant, meaning $c_v \approx c_p \approx c$. Because of constant specific heat, the internal energy formulation can be re-written as (Cengel, 2014):

$$\Delta U = mc_{avg}\Delta T \tag{2.4}$$

where:
m is the mass of the system
c_{avg} is the average specific heat
ΔT is the change in temperature

Energy transfer

Energy can be transferred either through heat transfer by a temperature difference, as mentioned previously or through work. Work can be a pump system, for example. The heat transfer is denoted Q, while for work, the symbol is W. Since the steel foundation is subject to a temperature difference, the energy will be transferred through heat movement; hence heat transfer will be the main focus.

While Q is the symbol for heat transfer for an entire process, $\dot{\mathbf{Q}}$ is the symbol for the heat transfer rate, where the dot mark denotes differentiation with respect to time. Q is the overall amount of heat during a given time interval Δt, and the following formula gives it

(Cengel, 2014):

$$Q = \int_0^{\Delta t} \dot{Q} dt \tag{2.5}$$

When $\dot{Q}$ is constant and the time variation is known, the equation becomes:

$$Q = \dot{Q} dt \tag{2.6}$$

where:

Q is the heat transfer

$\dot{Q}$ is the heat transfer rate

Δt is the change in time

The heat transfer rate through a given area is called heat flux and is given by:

$$\dot{q} = \frac{\dot{Q}}{A} \tag{2.7}$$

2.3 Steady state heat conduction

Conduction is the process where thermal energy is transmitted through a material when there is a difference in temperature. The conduction process is present in both liquids and gasses, as well as in solids. The heat transfer through conduction is given by the Fourier's law of heat conduction (Cengel, 2014):

$$\dot{Q}_{cond} = -kA\frac{\Delta T}{dx} = kA\frac{T_1 - T_2}{dx} \tag{2.8}$$

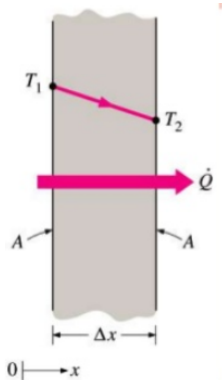

Figure 2.3: Heat conduction through a wall (Cengel, 2014)

In the equation 2.8 above, k is the thermal conductivity, and it is the ability of a material to conduct heat. A high thermal conductivity means that the material is efficient in conducting heat. In contrast, a low value of thermal conductivity means that a material is a poor conductor of heat and can serve as an insulator. An example of insulator material is the glass wool used in the walls of buildings (Cengel, 2014).

The second term in the equation is the area on which the heat transfer occurs, and the third term $\frac{\Delta T}{dx}$ is the temperature gradient. The temperature gradient is the slope of the tangent of the temperature curve at a given point, see figure 2.4.

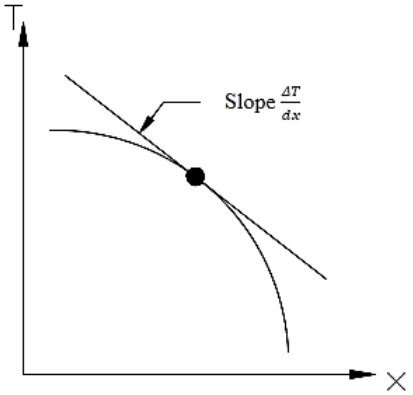

Figure 2.4: Temperature gradient (Cengel, 2014)

In equation 2.8 above, the heat transfer $\dot{Q}$ illustrated in figure 2.3 travels through the wall and the temperature drops as a result of the wall material resistance against the temperature. The equation 2.8 can be re-written as (Cengel, 2014):

$$\dot{Q}_{cond,wall} = \frac{T_1 - T_2}{R_{wall}} \tag{2.9}$$

and:

$$R_{wall} = \frac{L}{kA} \tag{2.10}$$

where:

$\dot{Q}_{cond,wall}$ is the heat transfer rate

T_1 and T_2 are the temperatures

R_{wall} is the resistance of the material against heat

k is the material conductivity

A is the area

L is the thickness of the wall

2.4 Steady state heat convection

The heat transfer through convection is done by the movement of fluid between areas of different temperatures. The heat transfer through convection is governed by Newton's law of cooling (Cengel, 2014):

$$\dot{Q}_{conv} = hA_s(T_s - T_\infty) \tag{2.11}$$

Similar to conduction equation 2.11 can be re-written as:

$$\dot{Q}_{conv} = \frac{T_s - T_\infty}{R_{conv}} \tag{2.12}$$

and:

$$R_{conv} = \frac{1}{hA_s} \tag{2.13}$$

Where:

$\dot{Q}_{conv}$ is the heat transfer rate through convection

T_s is the temperature of the solid surface

T_∞ is the ambient temperature

R_{conv} is the thermal resistance of the surface against heat convection

h is the convection coefficient

A_s is the solid surface area

Equation 2.13, where R is the thermal resistance, can be referred to as "the thermal resistance network" and is used when the heat is transferred in a system through both conduction and convection (Cengel, 2014). An example is the transfer of heat through a wall of a building. See figure 2.5.

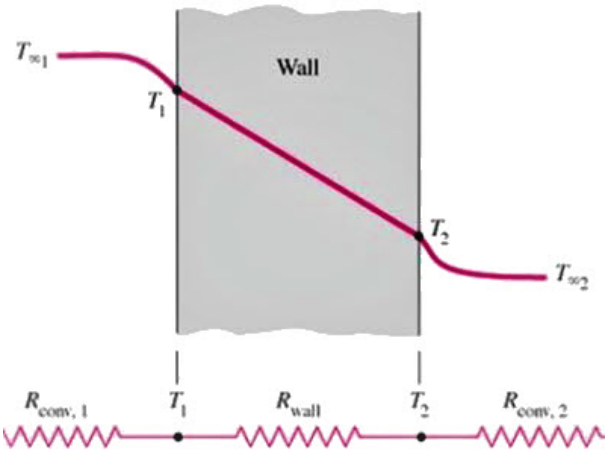

Figure 2.5: The thermal resistance network through a wall (Cengel, 2014)

The same principles of thermal resistance are applicable to the steel foundation, which is the subject of this thesis. For the steel foundation, there is convection from the air temperature both into the soil and into the hollow section, and conduction through steel, ice, water, and soil. Convection can be divided into two types, natural (or free) convection, and forced convection (Cengel, 2014).

2.4.1 Natural convection

Natural convection means that fluid moves only by natural means with no help from external factors. In general, fluid motion by natural convection is low, because the convection coefficient h from equation 2.11 above is also low. The convection coefficient h is defined as the rate of heat transfer between a solid surface and fluid. An example of natural convection is the heat transfer from a hot material to the surroundings. It is important to note that the heat transfer in the material is first by conduction and then

by convection to the surroundings (Cengel, 2014).

Figure 2.6 below presents an example of natural convection, the rise of a warmer fluid, and the fall of a cooler fluid.

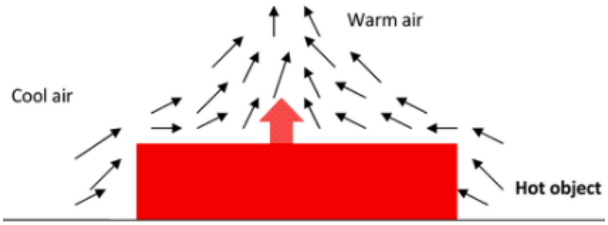

Figure 2.6: Example of natural convection (Cengel, 2014)

2.4.2 Forced convection

In forced convection, the fluid flow is forced over a surface or into a system by using an external force. The size of heat transfer thorough force convection is strongly dependant on the speed of the external forces. Higher velocity corresponds to a higher transfer rate. The flow caused by a fan is an example of forced convection. See figure 2.7.

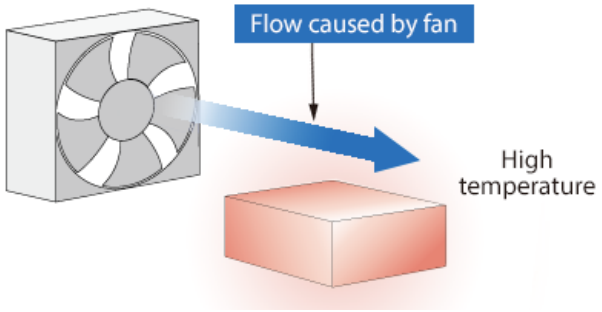

Figure 2.7: Example of forced convection (Cengel, 2014)

For the steel foundation, which is the subject of this thesis, both natural and forced convection mechanisms are present. First, there is natural convection from the air into the soil around the foundation. Further, there is also forced convection on the body of the circular section of the foundation because of the wind (Cengel, 2014).

2.5 Transient heat conduction

Steady-state heat conduction sets the basis for the theory behind transient heat conduction. As mentioned previously, in steady-state heat transfer, there is no variation of the

temperature inside the body at any time or at any position. The steel foundation can be analyzed using steady-state, but by doing so, we will only find the temperature at a specific time, and no information can be retrieved about temperature differences within the structure. In reality, the temperature varies with depth. The depth of the foundation is approximately 3 m. For finding the temperature of the foundation as a function of depth, a transient heat analysis is required. The first step in a transient heat analysis is to study the behavior of a system of which the interior temperature remains the same at any time during the heat transfer. In such a system, the temperature becomes a function of time, $T(t)$. This kind of analysis of a system is often referred to as a "lump system analysis."

For a lump system, the following expression applies based on energy conservation (Cengel, 2014):

Heat transfer into the body during dt = The increase in the energy of the body during dt

$$hA_s(T_\infty - T)dt = mc_p dT \tag{2.14}$$

With m=ρV and dT = d (T-T_∞), the equation 2.14 gives:

$$\frac{d\,(T - T_\infty)}{T - T_\infty} = -\frac{hA_s}{\rho V c_p}dt \tag{2.15}$$

Taking the integral of the expression 2.15 from t=0 to T=T_i the equation becomes:

$$ln\frac{T(t) - T_\infty}{T_\mathbf{i} - T_\infty} = -\frac{hA_s}{\rho V c_p}t \tag{2.16}$$

Taking the exponential of both terms, gives:

$$\frac{T(t) - T_\infty}{T_i - T_\infty} = e^{-bt} \tag{2.17}$$

where:

$$b = \frac{hA_s}{\rho V c_p} \tag{2.18}$$

The temperature of a lumped system at a given time or the time it takes for the lumped system to reach a specific temperature can be found with the equation 2.17. It is to be noted that a large value of b from equation 2.18 means that the lumped system will reach the ambient temperature in a short amount of time; the plot from figure 2.8 illustrates this. Additionally, b is proportional to the surface area but inversely proportional to the mass and the specific heat of the body.

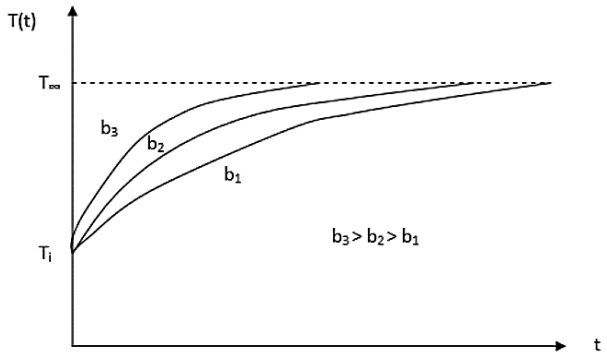

Figure 2.8: Temperature of the lump system (Cengel, 2014)

After finding the temperature of the lump system at a given time, the total amount of heat transfer between a body and its surroundings over a time interval can be found with the following formula:

$$Q = mc_p(T(t) - T_{\mathrm{i}}) \tag{2.19}$$

The lump system analysis described above can only be used when the following criterion is satisfied (Cengel, 2014):

$$B_i \leq 0,1 \tag{2.20}$$

where:

B_i is the biot number

h is the convection coefficient

k is the thermal conductivity

L_c is the characteristic length and is found by $L_c = \frac{V}{A_s}$

V is the volume

A_s is the surface area

B_i is called "biot number," which is dimensionless and gives the ratio of the heat transfer resistance. The Biot number takes into consideration the resistance of the system to heat convection and the resistance of the system to heat transfer through conduction (Cengel, 2014).

The lump system analysis is very helpful since it simplifies the problem by assuming that the temperature is not changing within the body of the system. The steel foundation has a length of approximately 3 m, and the temperature varies not only with time but also with the location, meaning that the temperature will be different at the surface compared to the bottom. When the foundation is filled with water, in wintertime, the water will freeze. The freezing depth is a critical factor. Finding exactly how much of the water will freeze gives the pressure that the foundation must withstand so that the circular section will not rupture.

2.5.1 Transient heat conduction in semi–infinite solids

A semi-infinite solid is a model that extends to infinity in all directions apart one. For example, the soil around the steel foundation can be considered as a semi-infinite solid. For a semi-infinite solid, an analytical solution that calculates the temperature near the surface can be developed. The analytical solution can then be used as a benchmark for the analysis done with the finite element software in a later chapter.

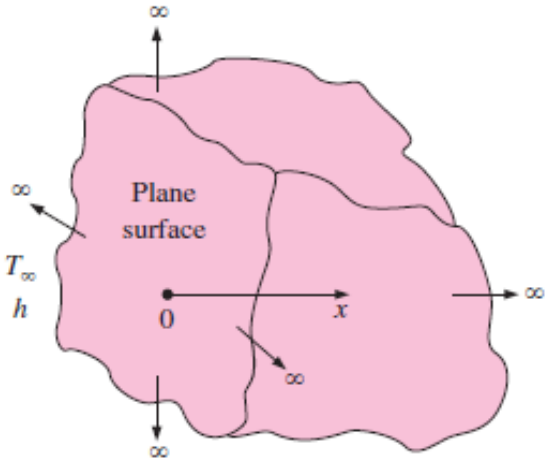

Figure 2.9: Illustration of a semi-infinite solid (Cengel, 2014)

In figure 2.9, we are interested in finding the heat transfer in x-direction if the surface temperature is T_s and the whole body has an initial temperature T_i. It is assumed that there is no heat generation in the body. Conductivity, density, and specific capacity are all constant (Cengel, 2014).

The energy equation gives:

$$\frac{\partial^2 T}{\partial x^2} + \frac{\partial^2 T}{\partial y^2} + \frac{\partial^2 T}{\partial z^2} + \frac{e_{gen}}{k} = \frac{1}{\alpha}\frac{\partial T}{\partial t} \tag{2.21}$$

From the assumption made above, since it is only considered heat transfer in the x-direction and no internal heat generation, the energy equation becomes:

$$\frac{\partial^2 T}{\partial x^2} = \frac{1}{\alpha}\frac{\partial T}{\partial t} \tag{2.22}$$

Boundary conditions: $T(0,t) = T_s$

Initial conditions: $T(x,0) = T_i$. At any position x inside the body at $t = 0$, the temperature is T_i.

The partial derivation can be solved by converting it into an ordinary differential equation. This is done by changing the two variables x and t into a similarity variable called η, which is defined as:

$$\eta = \frac{x}{\sqrt{4\alpha t}} \tag{2.23}$$

By using the chain rule, equation 2.22 gives:

$$\frac{\partial T}{\partial t} = \frac{dT}{d\eta}\frac{\partial \eta}{\partial t} = \frac{-x}{2t\sqrt{4\alpha t}}\frac{dT}{d\eta} \tag{2.24}$$

$$\frac{\partial T}{\partial x} = \frac{dT}{d\eta}\frac{\partial \eta}{\partial x} = \frac{1}{\sqrt{4\alpha t}}\frac{dT}{d\eta} \tag{2.25}$$

$$\frac{\partial^2 T}{\partial x^2} = \frac{d}{d\eta}\left(\frac{\partial T}{\partial x}\right)\frac{\partial \eta}{\partial x} = \frac{1}{4\alpha t}\frac{d^2 T}{d\eta^2} \tag{2.26}$$

By substituting the answer from equation 2.26 into equation 2.22 and after simplification, gives:

$$\frac{d^2 T}{\partial \eta^2} = -2\eta\frac{dT}{d\eta} \tag{2.27}$$

Equation 2.27 is an ordinary differential equation of second order with only one variable η. Further the equation can be solved by defining a new variable:

$$w = \frac{dT}{d\eta} \tag{2.28}$$

Furthermore equation 2.27 is converted into a first order differential equation by substituting the new defined variable w:

$$\frac{dw}{d\eta} = -2\eta w \tag{2.29}$$

In equation 2.29 by re-arranging the variables and integrating, gives:

$$\frac{dw}{w} = -2\eta d\eta \tag{2.30}$$

$$ln\ w = -\eta^2 + C_0 \tag{2.31}$$

Taking the exponential, the solution is:

$$w = C_1 e^{-\eta^2} \tag{2.32}$$

where:

$$C_1 = lnC_0 \tag{2.33}$$

Equation 2.32 is now substituted back into equation 2.28

$$\frac{dT}{d\eta} = C_1 e^{-\eta^2} \tag{2.34}$$

$$dT = C_1 e^{-\eta^2} d\eta \tag{2.35}$$

Taking the integral in equation 2.35 gives:

$$T = C_1 \int_0^{\eta} e^{-u^2}\ du + C_2 \tag{2.36}$$

Now solving for C_1 and C_2 with the following boundary conditions, gives:

BC1: At $\eta = 0$, gives C_2=T_s

BC2: $\eta \to \infty$, gives T_i=C_1

$$T_i = C_1 \int_0^{\infty} e^{-u^2} du + C_2 = C_1 \frac{\sqrt{\pi}}{2} + T_s \to C_1 = \frac{2(T_i - T_s)}{\sqrt{\pi}} \tag{2.37}$$

By substituting C_1 and C_2 in equation 2.36 gives:

$$\frac{T - T_s}{T_i - T_s} = \frac{2}{\sqrt{\pi}} \int_0^{\eta} e^{-u^2} du = erf(\eta) = 1 - erfc\,(\eta) \tag{2.38}$$

Where $erf(\eta)$ is the error function, and $1 - erfc(\eta)$ is the complementary error function.

The integral from equation 2.38, cannot be solved analytically only numerically; hence the function $erf(\eta)$ is evaluated numerically for different values of η. The term is similar to sinus and cosine function, which also cannot be solved analytically. It is the result of a numerical solution.

The graph in figure 2.10 gives different values for η.

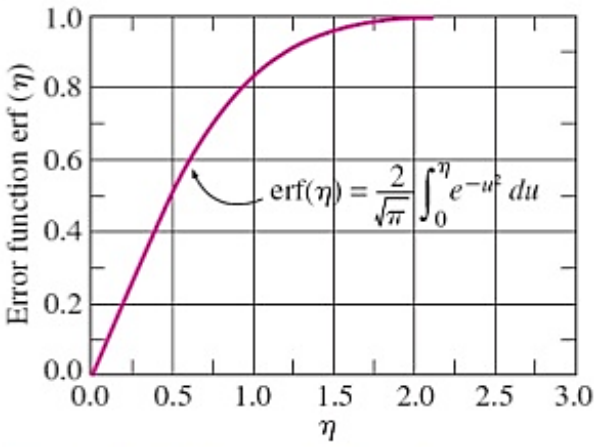

Figure 2.10: Error function (Cengel, 2014)

Using the graph from figure 2.10 the error function value wouldn't be very accurate, a calculator can be used to get accurate values.

Now, by substituting 2.23 in to 2.38 the temperature distribution for a surface with constant temperature is given by the following equation (Cengel, 2014):

$$\frac{T(x,t) - T_i}{T_s - T_i} = erfc\left(\frac{x}{\sqrt{4\alpha t}}\right) \tag{2.39}$$

where,

T_s is the surface temperature

T_i in the initial temperature of the system

α is thermal diffusivity and is equal to $\alpha = \frac{k}{\rho c_p}$

x is the depth measured from the surface

t is the time

$T(x,t)$ is the temperature of the body at a given location and time

$erfc(\eta)$ is the complimentary error function

Equation 2.39 has been presented for comparations purposes. In a later chapter, a benchmark of finite element analysis versus an analytical solution will be presented.

3 Thermal analysis

Three thermal analyses have been performed. First, two models were conducted to verify the results received from the finite element analysis simulation. For the first model, an analytical solution is possible based on the heat transfer theory previously described. Furthermore, for the second model, more complexity was added, including non–linearity of the heat transfer mechanism. The third analysis is a model of the foundation filled with water for calculating the depth of the ice plug.

All models have been carried out using Abaqus/CAE 2019, a general-purpose finite element program. All models are built as axis-symmetric models.

An axisymmetric analysis significantly reduces the computation time and the modeling time, it requires smaller input and gives a smaller output file (Alavala, 2008).

The models are presented in the following order:

1. Model of soil without foundation with linear heat transfer to be validated with an analytical solution
2. Model of soil without foundation with non-linear heat transfer to calculate the soil frost depth, benchmark against the values given in "451.021 Klimadata for termisk dimensjonering og frostsikring" (Byggforskserien, 2018)

3. Model of the steel foundation in soil filled with water for analyzing the amount of water that freezes

For all analyses the sides of the models are insulated, i.e., no horizontal heat transfer is allowed, as only vertical heat transfer is considered. This implies that the soil conditions in the considered area are reasonably homogeneous, i.e., the model is far from large rocks and buildings. Furthermore, the bottom end is also insulated (adiabatic) since the temperature at this level is not known. In order to avoid boundary condition effects in the upper 2-3 (m), the model is built 10 (m) deep and with a radius of 4 (m).

3.1 Linear soil analyses

This model was built to verify the analysis methodology by comparing it to an analytical solution. The analytical solution is based on the theory studied in subsection 2.5.1 of the thesis.

3.1.1 Input parameters

For performing the calculations and the simulation several parameters are required. For this analysis the input parameters were taken from the available literature. The parameters have been chosen for a random soil type since the analysis is only for comparing the analytical solution with the methodology used to build the FE-model. All parameters are given in table 3.1. Please note that SI units for temperature is Kelvin degrees and, for making it more convenient for the reader to follow, the temperature is converted into Celsius degrees.

Table 3.1: Data for linear analysis of soil

Materials	Specific heat (J/kgK)	Conductivity (W/mK)	Density (kg/m^3)	Initial temperature (°C)	Surface temperature (°C)
Soil	1480	2,5	2000	0	20

3.1.2 Analytical solution

The equation developed in subsection 2.5.1 is applied to check the FE-model against the analytical solution. Equation 2.39 is used to find the temperature of the soil at different depths. The formula assumes a constant initial and surface temperature. The equation also takes into consideration for how long the surface temperature is applied, in terms of time. Further, the temperature at a specific location is calculated by taking into account the thermal diffusivity. Thermal diffusivity measures the rate at which heat spreads throughout the material. The equation can't be used if non–linearities are introduced, for example, if the conductivity is a function of temperature. An example is presented below to clarify how the temperature at a specific point and time is found by using the equation 2.39.

In the example below, the temperature at a depth of 0,5 (m) after a period of 7 days is found. In order to stay consistent with the units the days are converted into seconds.

$$\frac{T(x,t) - T_i}{T_s - T_i} = erfc\left(\frac{x}{\sqrt{4\alpha t}}\right)$$

$$\alpha = \frac{2,5}{2000 \cdot 1480} = 8,45 \cdot 10^{-7} m^2/s$$

$$\eta = \frac{0,5}{\sqrt{4 \cdot 8,45 \cdot 10^{-7} \cdot 604800}} = 0,350$$

Knowing the value of η the complementary error function is:

$$erfc(\eta) = 0,621$$

All variables are known, by substituting, the temperature at 0,5 (m) after 7 days (604800 s) is found:

$$T(0,5; 604800) = 0,621 \cdot (293,15 - 273,15) + 273,15 = 285,56°K = 12,41°C$$

In the appendix A1, the temperature is calculated in the same manner to a depth of 3,5 (m).

3.1.3 Model setup for the finite element analysis

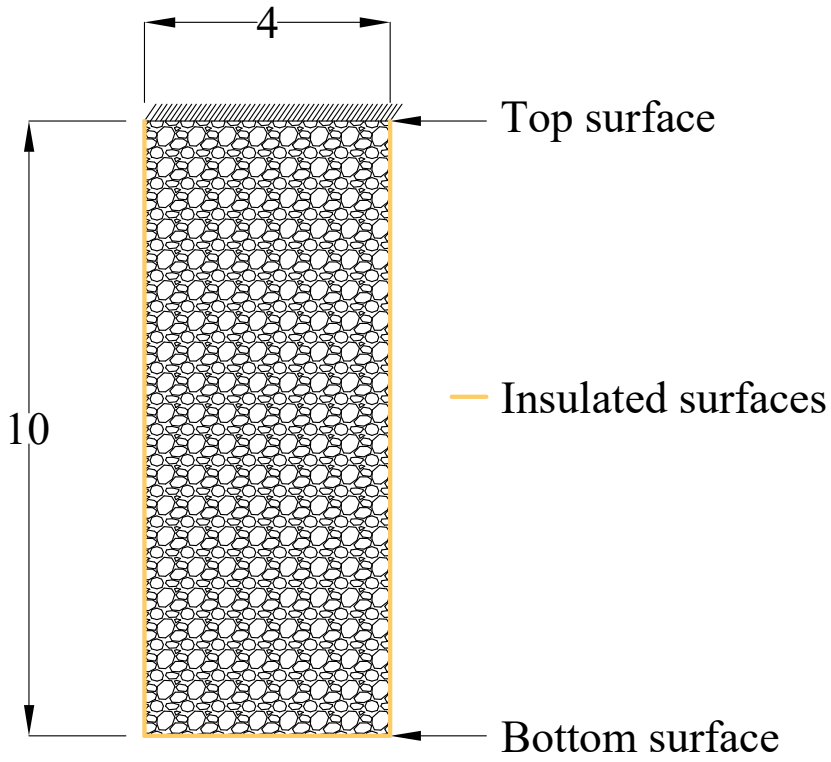

Figure 3.1: Model setup of the soil for the linear analysis (dimensions in m)

In this chapter, a simple model is created to be checked against the analytical solution. The model is an important first step to the more advanced simulation needed in order to find out the depth of the ice plug that can be formed in the steel foundation. In figure 3.1, the model is illustrated. The model represents the pit in which the steel foundation is placed. The pit has a 10 (m) height and a radius of 4 (m). The simulation aims to find the temperature inside the soil at different depths, in the same manner as the analytical solution from the previous subsection. The same parameters used in the analytical solution are used again here, see table 3.1 above. In Abaqus, this is a transient heat transfer problem because the temperature is a function of position inside the soil, meaning that the temperature will be different deeper in the soil. The heat transfer through soil is in the y-direction, in the vertical direction only. In this case, the applied surface temperature is higher than the initial temperature of the soil, meaning the heat transfer will be from top to bottom. The heat transfer is through conduction only. The outer surfaces of the soil are fully insulated; there is no heat loss, see figure 3.1. The element mesh size has been

set to 250x250 (mm), which is indeed a coarse mesh, but this is enough for the purpose of comparing it against the analytical solution.

3.1.4 Results and discussion

The FEA has been verified by comparing it with the values found from the analytical solution. Based on the input data, the temperatures at different depths were found after a period of 7 days while holding a constant surface temperature of 20 (°C).

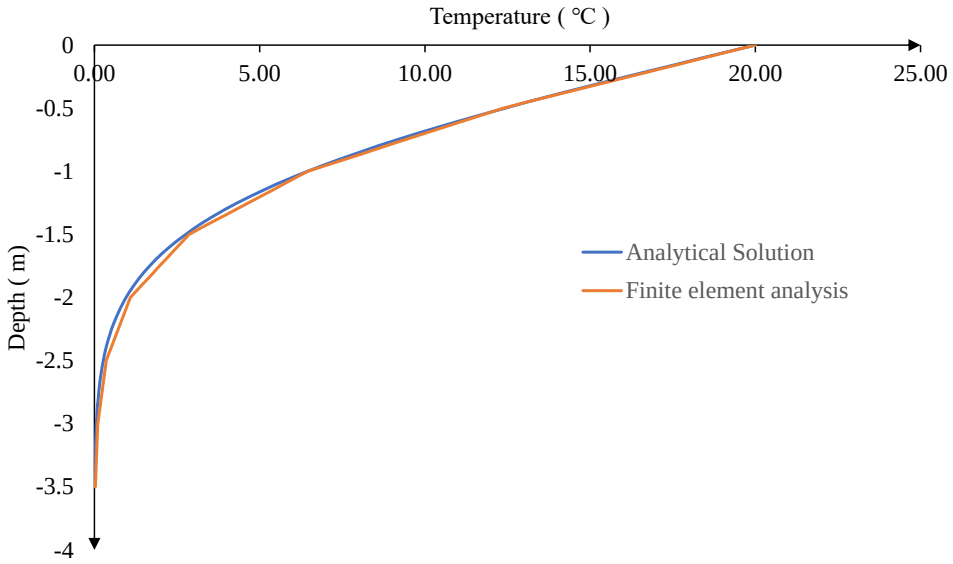

Figure 3.2: Comparison of temperature-depth relation between the analytical solution and the FE-model

Figure 3.2 shows that the analytical solution gives very close results in comparison with the FE-analysis. As mentioned before, the analysis does not involve any nonlinearities; hence a convergence is easily achieved by Abaqus.

The plot shows how the temperature drops with depth. The slopes for both curves are steep in the beginning and are flattened after a distance of approximately 2 (m).

After 2 (m), the temperature doesn't quite reach deep in the soil; as a result, the temperature stays close to the initial temperature given in the input. Closer to the surface, both solutions are approximately identical, but deeper into the soil, the difference is increasing. Notice that the curve from the finite element analysis between 1 and 2,5 (m) depth it is not as smooth. This is a result of the mesh choice.

In this case, the coarse mesh gave a very short computational time while providing close results for comparison. Refining, the mesh and the use of smaller increments will result in less discrepancy between the solutions and a smoother curve for the simulation. As seen from the diagram, the analytical solution converges well with the simulation. More complexity can now be incorporated into the simulation.

3.2 Nonlinear soil analysis

The first model was built to verify the analysis methodology by comparing it to the analytical solution given by equation 2.39. The model was relatively simple without nonlinearities. Further, in this section, a new model is built to verify the analysis methodology by comparing it to the tubular frost depth values given in Byggdetaljer 451.021 (Byggforskserien, 2018).

3.2.1 Input parameters for the nonlinear soil analysis

In this subsection, the parameters used in the simulation conducted in Abaqus CAE are provided and explained.

3.2.1.1 Conductivity

In the theory chapter, the conduction was defined as the process where thermal energy is transmitted through a material when there is a difference in temperature. In table 3.2, the conductivity of both frozen and unfrozen soil is presented (Byggforskserien, 2018).

Table 3.2: Conductivity data

Conductivity (W/mK)	Temperature (°C)
2,50	-30,00
2,50	-1,00
1,50	0,00
1,50	30,00

Conductivity is divided as temperature-dependent. The nonlinear conductivity reflects the phase change from water to ice and back again. The conductivity given in table 3.2 is graphically presented in figure 3.3.

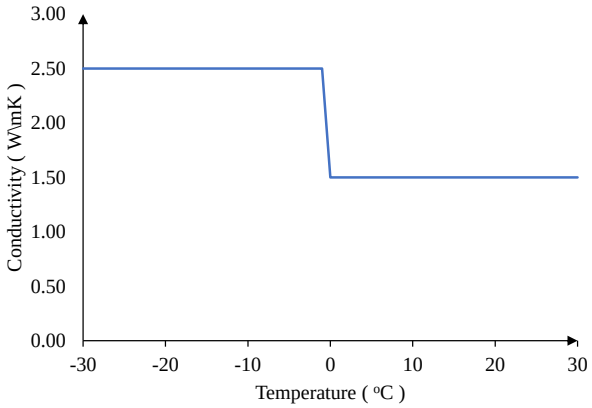

Figure 3.3: Temperature-conductivity relation

In figure 3.3 is shown how the finite element software is handing the input data given for the conductivity. As mentioned, the conductivity, in this case, is temperature-dependent. Abaqus CAE is using a conductivity of 1,50 (W/mK) when the applied temperature is between 0 (°C) to 30 (°C) and 2,50 (W/mK) if the temperature is subzero.

Observe the slope of the curve when the conductivity and temperature values are changing. Not to run into convergence issues, a slight slope is introduced. This way is easier for the software to increment, reducing cutbacks and making the computational time shorter.

3.2.1.2 Volumetric heat capacity and specific heat

The finite element software used for the simulation doesn't have a built-in volumetric heat capacity function. Specific heat c_p and the volumetric heat capacity C of a material represents the heat storage capability. The volumetric heat capacity is expressed per unit volume, while the specific heat is expressed per unit mass. The volumetric heat capacity is given in Byggdetaljer 451.021 (Byggforskserien, 2018) and is converted to specific heat. Specific heat is used as an input in Abaqus.

The conversion is made with equation 3.1 (Cengel, 2014).

$$C = \rho c_p \tag{3.1}$$

where:

C is the volumetric heat capacity

ρ is the total density

c_p is the specific heat (at constant pressure)

The specific heat is found for both frozen and unfrozen soil state and given in the table 3.3.

Table 3.3: Volumetric heat capacity and specific capacity input

Volumetric heat capacity (J/m^3K)	Specific heat (J/kgK)	Soil state
$1{,}90 \cdot 10^6$	1055,56	Frozen
$3{,}00 \cdot 10^6$	1666,67	Unfrozen

3.2.1.3 Latent heat

The latent heat is the energy absorbed or released by a material during a phase change or, in other words, a change during its physical state that occurs without any change in temperature. In this case, from liquid to solid. The latent heat of soil is calculated with the following equation (French, 2017):

$$L = \rho \, wL_w \tag{3.2}$$

where:

L is the latent heat of soil when the phase change occurs

ρ is the dry density of the soil

w is the water content in percent

L_w is the latent heat of water

The density and water content are dependent on the soil type while the latent heat of fusion for water is always the same (Mellor, 1977). Byggdetaljer 451.021 gives the following values for frost susceptible soils (Byggforskserien, 2018):

Table 3.4: Density, water content and latent heat of water

Density (kg/m^3)	Water content (%)	Latent heat of water (J/m^3)
1350	33%	$334 \cdot 10^6$

Based on the data from table 3.4 the latent heat for soil is calculated with equation 3.2:

$$L = 1350 \cdot 10^{-3} \cdot 0,33 \cdot 334 \cdot 10^{6} = 150 \cdot 10^{6} J/m^{3}$$

Byggdetaljer 451.021 confirms the value of 150·10^6 (J/m^3) found by using equation 3.2 above (Byggforskserien, 2018).

When the water in the soil freezes, the conductivity, volumetric heat, and the specific heat changes. As a result, latent heat is released. Simulating the phase, change from liquid to solid can be done in different ways. In this simulation, the latent heat is modeled by increasing the specific heat capacity of the soil between 0 (°C) to -1 (°C), see table 3.5.

Table 3.5: Specific heat input data

Specific heat (J/kgK)	Temperature (°C)
1055,56	-30,00
1055,56	-1,005
85000,00	-0,995
85000,00	-0,005
1666,67	0,005
1666,67	30,00

This approach is supported by NS-EN 13793 (ISO, 2001). For soil, the value of 85000 (J/kgK) is added to the specific heat capacity curve, giving an extra heat of 150·10^6 (J/m^3) required to reduce the temperature by one-degree (°C). The table 3.5 is graphically represented in figure 3.4. The temperature is plotted only between -2 and 2 degrees to show more clearly exactly where the specific heat changes. A slope is introduced here as well for the same reason previously explained, see subsection 3.2.1.1.

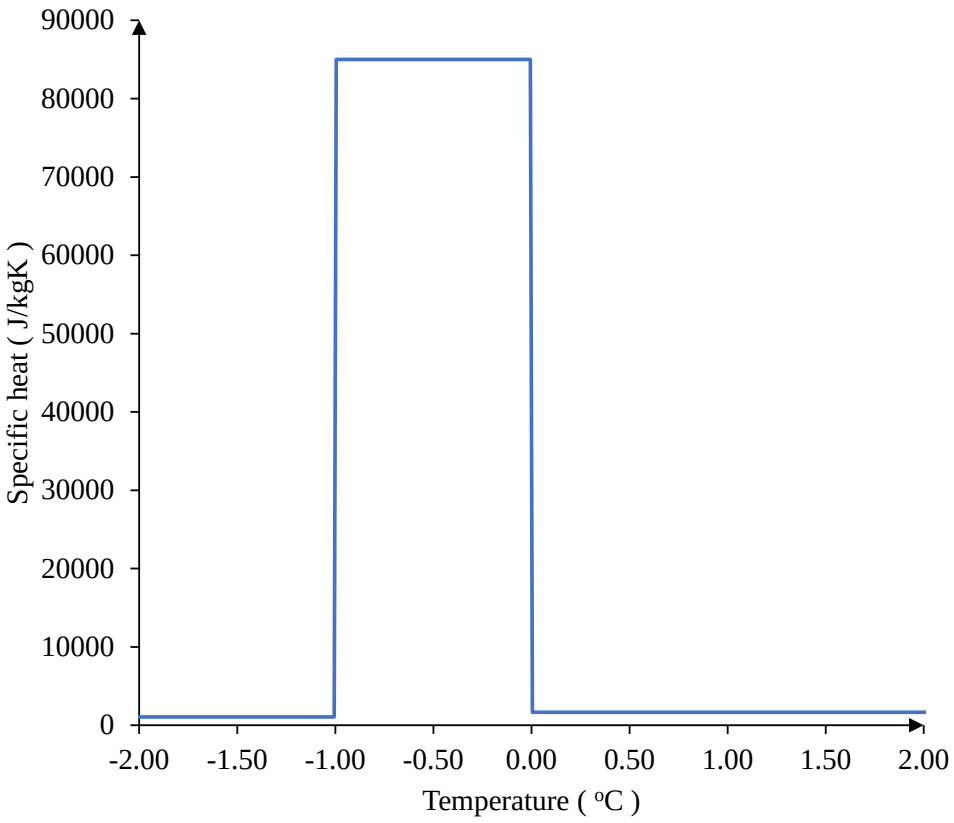

Figure 3.4: Specific heat-temperature relation

Figure 3.5 shows graphically how Abaqus CAE is processing the latent heat from the specific heat and temperature (Hibbitt et al., 1997).

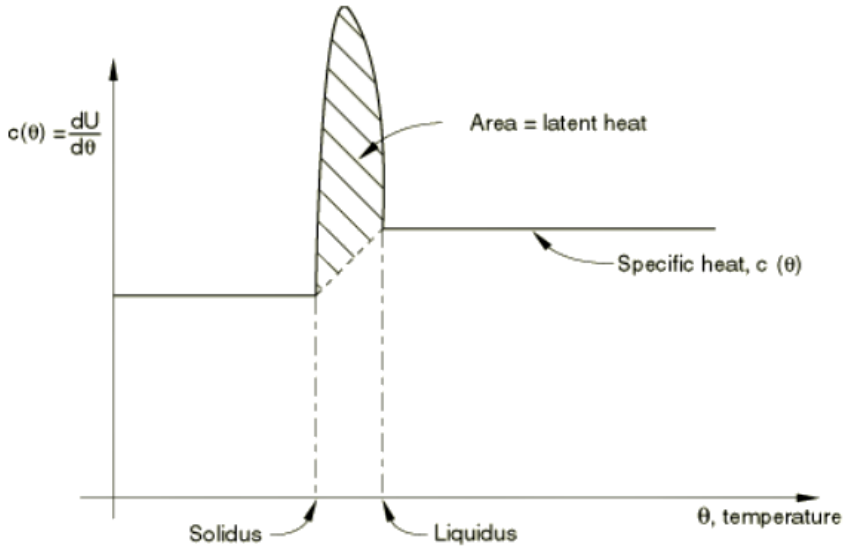

Figure 3.5: Specific heat, latent heat definition (Hibbitt et al., 1997)

As shown in figure 3.5, the latent heat is modeled by increasing the specific heat capacity

of the soil over a temperature difference (Hibbitt et al., 1997). By taking into consideration latent heat, the specific heat table previously given is extended. See table 3.5 above.

3.2.1.4 Temperature data

For the first project, Statnett has begun using the steel foundations in the North of Norway, more specifically in the area of Alta; hence the temperature is set accordingly. The initial temperature of the soil is equal to the annual mean. "Loading" is applied as a surface temperature time series at the top nodes of the model.

The time series is defined as a sine curve that cycles about the annual mean temperature. It starts at 21.03.2019 (Equinox) and ends at 04.05.2021, as shown in figure 3.6. The frost depth is then found at the end of the second winter season.

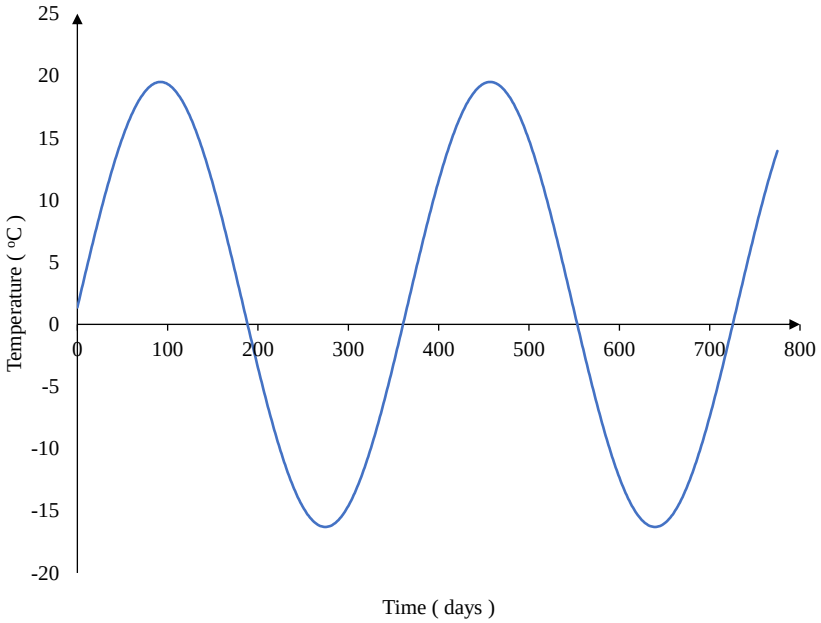

Figure 3.6: Temperature for Alta, T_{mean}=1,6 (°C) and T_{ampl}= 17,9 (°C)

Note that the sine curve parameters are given in (Byggforskserien, 2018), i.e., temperature mean and amplitude, define a 100-year return period.

3.2.2 Analytical solution

In Byggdetalj 451.021, the frost depth is given for a range of locations in Norway. The frost depth is based on 100-year return period and is calculated with the following equation (Byggforskserien, 2018):

$$H_0 = \sqrt{\frac{7200 F_d \lambda_f}{L + C\Theta_m}} \tag{3.3}$$

The frost depth for Alta is:

$$H_0 = \sqrt{\frac{7200 \cdot 43000 \cdot 2,5}{150 \cdot 10^6 + 3 \cdot 10^6 \cdot 1,6}} = 2,24m$$

where:

F_d is the design freezing index. For Alta F_d= 43000 h°C (Byggforskserien, 2018)

λ_f is the conductivity of the frozen ground ref. table 3.2

L is the latent heat of freezing for soil given previously

C is the volumetric heat capacity ref. table 3.3

Θ_m is the annual mean temperature. For θ_m= 1,6 °C (Byggforskserien, 2018)

The values for calculating the frost depth have been validated by experimental data from actual constructions and have been used in Nordic countries over many years with satisfactory results in preventing frost heave (ISO, 2001) (Byggforskserien, 2018).

The analytical solution to the problem is 2,24 (m).

3.2.3 Model setup for the finite element analysis

As in the previous analysis, the dimensions of the soil are unchanged and the model is 2D axis-symmetric. The model represents the soil in which the steel foundation is placed and buried. The model geometry is 10 (m) height and 4 (m) long, figure 3.7. The foundation is approximately 3 (m) high and the geometry of the soil is chosen to avoid the boundary conditions effects in the upper 3 (m) where the foundation is placed.

The soil is assumed to be fully saturated; hence the values for specific heat, conduction, and density were chosen accordingly. The heat transfer through soil is one dimensional, in the vertical direction only. This implies that the soil conditions are reasonably homogenous, i.e., the model is far from large rocks, buildings, etc. Since the only material is wet soil, the heat transfer is through conduction only.

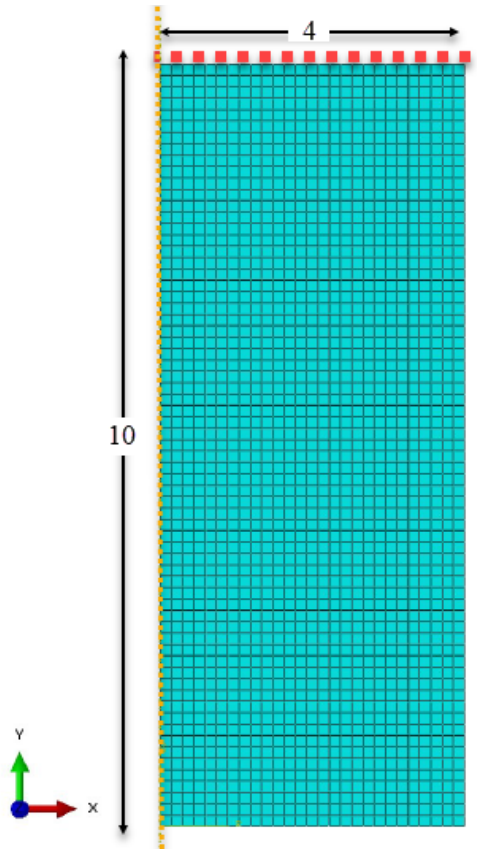

Figure 3.7: Meshed model setup for the nonlinear analysis (dimensions in m)

The temperature is applied on the surface of the soil (red squares in figure 3.7) with a given initial temperature. The mesh size is set to 150x150 (mm), like in the previous simulation. The dimensions of the mesh size are based on computation cost and accuracy. Since this is a validation model, we are only interested in checking the maximum frozen depth of the soil by comparing it with the analytical solution from the previous section. The small variations in temperature inside the soil are not of interest here, only the maximum frozen depth; hence a finer mesh is not needed. The time increments in the FE analyses are set to ensure that the non-linearities are properly handled. A time step of 86400 seconds (1 day) is used, for which the maximum temperature change is roughly 0,5 (°C). In this way, the non-linear heat capacity between 0 (°C) and -1 (°C) is well handled.

3.2.4 Results and discussion

The analysis model has been verified by comparing it with the analytical solution from section 3.2.2. Table 3.6 summarizes the results.

Table 3.6: Results comparison

Solution	Return period	Frost depth (m) at T:		Percent error at T:	
		-0.1 (°C)	-1 (°C)	-0.1 (°C)	-1 (°C)
FE-model	100-year	2,34	1,9	4,4%	15,1%
Analytical		2,24			

The maximum frost depth is taken at the time just before it starts to melt from the top and the end of the second winter period. Two values are given in table 3.6, one when the temperature profile intersects -0.1 (°C) and one where it intersects -1 (°C). Those values are chosen since ice starts to form at 0 (°C) but is not completely formed until -1 (°C).

Note the modeling of latent heat, where the specific heat capacity is increased between 0 (°C) and -1 (°C). This means that latent heat is not fully generated until the temperature reaches -1 (°C), for the temperature in between water and ice can be viewed as existing together.

Physically, a temperature of -1 (°C) is most accurate, where all the water has turned to ice. However, it is evident that the analytical solution agrees better with the temperature limit of -0.1 (°C). It appears that the values given in Byggdetaljer 451.021 are chosen to be on the conservative side, thus frost depth is given down to a level where ice has started to form.

The analysis methodology used to simulate the maximum frozen depth of the soil has shown to correlate reasonably well with the frost depth given by the empirical equation and the values specified by Byggdetaljer 451.021. The relatively small difference between the values (percent error 4,4%) is assumed to be because of two different calculations approaches.

Having confirmed that the analysis methodology gives trustworthy results, the same analysis methodology will be used in the next chapter to evaluate the amount of ice that can be formed inside the steel foundation.

3.3 Analysis of the steel foundation

The steel foundation developed by Statnett may be situated in areas with high groundwater, where low temperatures can lead to ice formation inside the hollow vertical section. In

this section, a thermal analysis is presented, performed to evaluate the amount of ice that can be formed inside the hollow section when this is assumed to be filled with water at the ground level. The simulation is done based on the same analysis methodology previously presented.

3.3.1 Input parameters for the steel foundation

In addition to the soil properties evaluated earlier, parameters for steel and water are added to the simulation.

3.3.1.1 Conductivity

The conductivity parameters for soil are unchanged. For steel, the conductivity is chosen based on the steel quality of the foundation (Cengel, 2014). Ice has a different conductivity than water. Furthermore, the conductivity is dependent on the temperature. The graph under shows how conductivity of water and ice varies with the temperature (Melinder, 2007; Ramires et al., 1995).

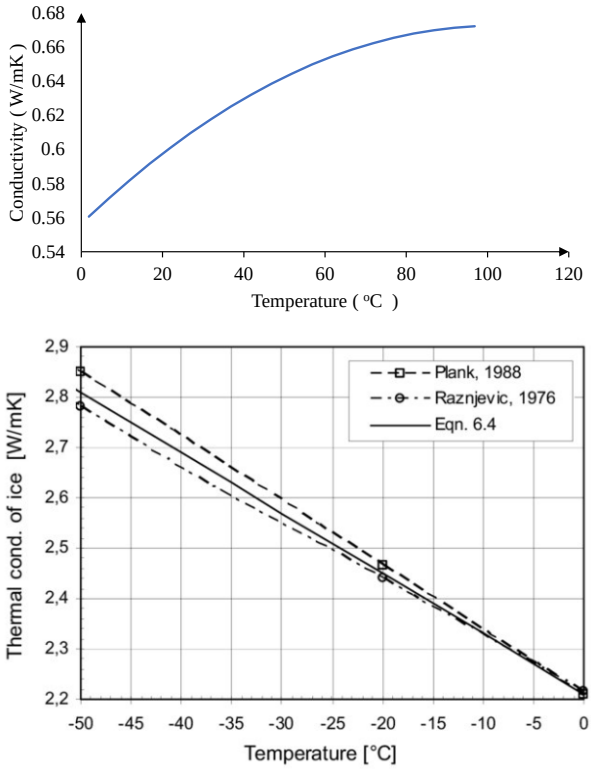

Figure 3.8: Thermal conductivity of ice and water as function of temperature (Melinder, 2007; Ramires et al., 1995)

Based on the plots from figure 3.8 an average value for the conductivity of water and ice was chosen with respect to the temperature intervals at which the steel foundation is subjected. It is important to note that water transports heat most efficiently by convection. However, conduction can become the dominant heat flow in the steel foundation. This requires a higher density at the bottom than at the top. In a situation where the bottom layers hold between 1 and 4 (°C), while the top layers hold close to 0 (°C), convection is reduced to a minimum.

The non–linear conductivity given in table 3.7 reflects the phase change from water to ice and back again.

Table 3.7: Thermal conductivity data for water and ice

Materials	Conductivity (W/mK)	Temperature (°C)
Water/Ice	2,30	-30,00
	2,30	-1,00
	0,61	0,00
	0,61	30,00
Steel	60,50	

3.3.1.2 Density

From figure 3.9 it can be seen how the density is fluctuating with the change in temperature, notice how water has the maximum density when the temperature reaches 4 (°C) (Melinder, 2007).

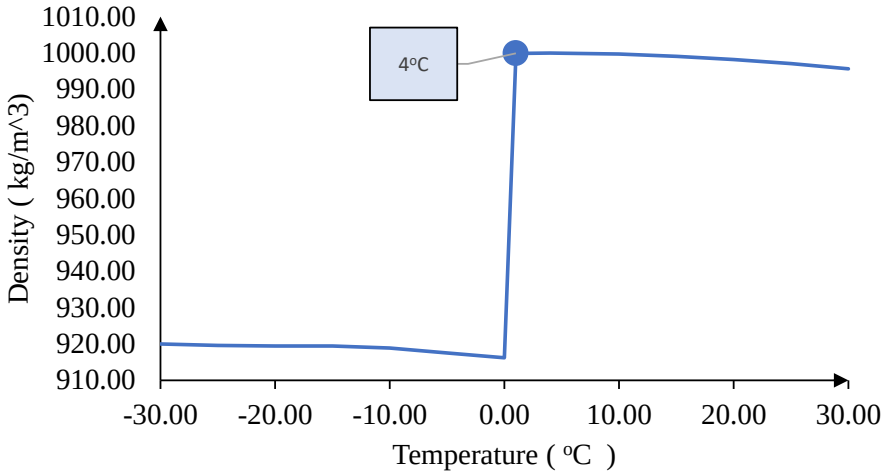

Figure 3.9: Density of ice and water as a function of temperature (Melinder, 2007)

The density of water and ice changes with temperature, an average density value for ice, and another for water has been selected based on the temperature. The density of steel was chosen based on the S355 strength class of the steel foundation.

Table 3.8: Density parameters

Material	Density (kg/m^3)
Water	1000
Ice	918,28
Steel	7850

For the soil, the density is unchanged. The same values are used as in the previous simulation.

3.3.1.3 Volumetric heat capacity and specific heat

The specific heat for water is calculated from the volumetric heat capacity in the same manner as in the previous model by using equation 3.1. For soil, the parameters are unchanged, while for steel, the specific heat reflects the chemical composition of the structural steel grade (ISO, 2001; Cengel, 2014).

Table 3.9: Volumetric heat capacity and specific capacity input for the foundation

Material	Volumetric heat capacity (J/m^3K)	Specific heat (J/kgK)
Water	$4{,}18 \cdot 10^6$	2048,39
Ice	$1{,}88 \cdot 10^6$	4180,00
Steel	N/A	434,00

3.3.1.4 Latent heat

For water, the latent heat is modeled by increasing the specific heat capacity between 0 (°C) and -1 (°C) in the same way as in the previous analysis. Here are as well the soil parameters are unchanged.

Table 3.10: Specific heat input for water and ice

Specific heat (J/kgK)	Temperature (°C)
2048,39	-30,00
2048,39	-1,005
338180,00	-0,995
338180,00	-0,005
4180,00	0,005
4180,00	30,00

3.3.1.5 Film coefficient

The film's coefficient or convection coefficient is defined as the heat transfer rate between a solid surface and a fluid. In general, convection can be of two types, natural or forced convection. Both were explained in the theory chapter.

For the steel foundation, two film coefficients are required, one for free convection and one for forced convection. The highest value of the film coefficient is valid for forced convection (by wind), whereas the lower value represents the interior of the foundation hence it is natural convection. See table 3.11

Table 3.11: Film coefficients parameters

Material	Film coefficient (W/Km^2)	Type of convection
Soil	25	Forced
Water	10	Natural
Steel inside	10	Natural
Steel outside	25	Forced

It is difficult to assign a film coefficient because h is an experimentally determined parameter and depends on properties like surface geometry, nature of fluid motion, properties of the fluid, fluid velocity and the inclination of the surface (Bai and Bai, 2010). The film coefficients used on the simulation are based on typical values found in (John

et al., 2006). These values were crosschecked with other different sources and have been found to converge well.

3.3.1.6 Temperature

The surface temperature is applied at the top nodes, as it was done in the previous soil model. Also, for this analysis, the body of the foundation and the water inside it are also subjected to the same surface temperature. Two temperatures scenarios are analyzed.

In the first scenario, the surface temperature represents the average day temperature recorded in Alta over a period of two years. The winters in which the temperatures are lowest are used from the available data provided by the meteorological institute. The input surface temperature is plotted, and it can be seen in figure 3.10 below (institutt, 2020).

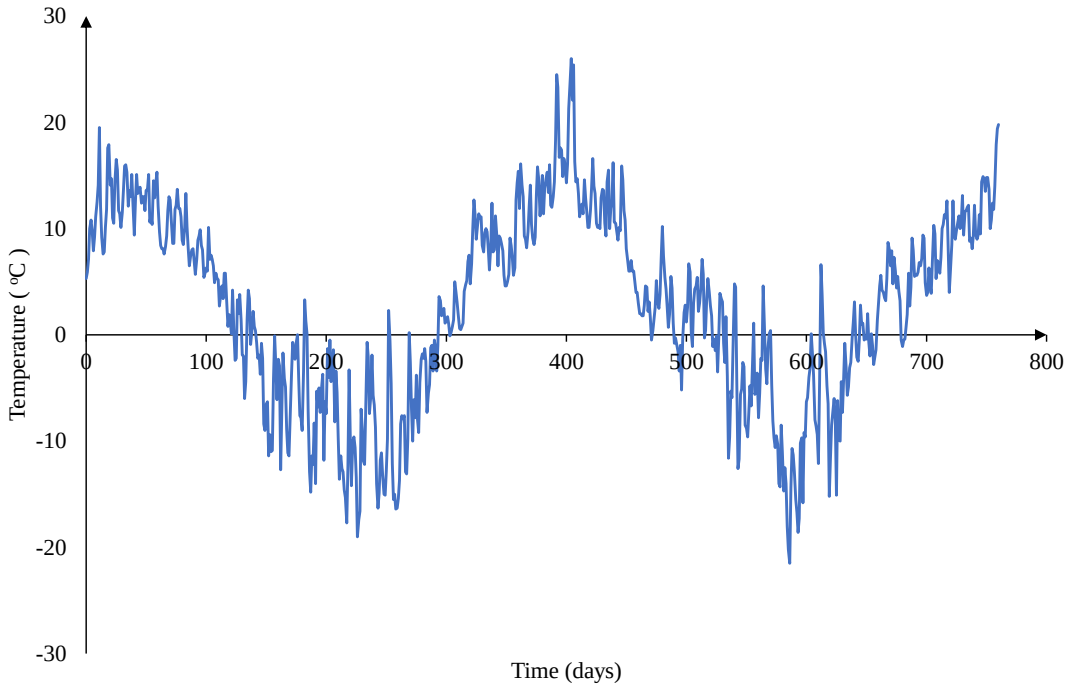

Figure 3.10: Average day temperature in Alta over a period of 760 days

The local recorded temperatures give a good representation of the actual conditions from the site where the foundations are placed.

In the second scenario, the applied surface temperature is the one from the previous simulation representing a 100-year return period (Byggforskserien, 2018).

The hole model has been given an initial temperature of $T_{mean} = 1{,}6$ (°C) which represents the annual mean temperature for Alta.

3.3.2 Model setup for the finite element analysis

The FE-model is an axis-symmetric model with a 4-node linear axisymmetric heat transfer quadrilaterals. The first two models previously presented were built to verify the analysis methodology by comparing it with the available analytical solutions.

This model was built nearly with the same boundary conditions and the same soil properties as the second model but with water, ice and steel included.

The right, left, and bottom sides of the model are insulated, i.e., no horizontal heat transport is allowed, as only vertical heat transport is considered. As in the previous models it is assumed that the model is far from large rocks and other obstacles. To avoid boundary conditions effects in the upper 2-3 (m), the model is built 10 (m) deep and with a radius of 4 (m).

Note that the steel pad is not modeled; this is because the pad connected to the hollow steel section is considered to have a negligible effect on the formation of ice inside the tubular section.

In figure 3.11 the axis-symmetric model of the foundation is presented. The figure to the left gives an overview of the model, while the one to right presents a closer view of the upper side of the model. In addition, for better understanding, Abaqus CAE can render a 3D-view of the axis-symmetric model, see figure 3.12.

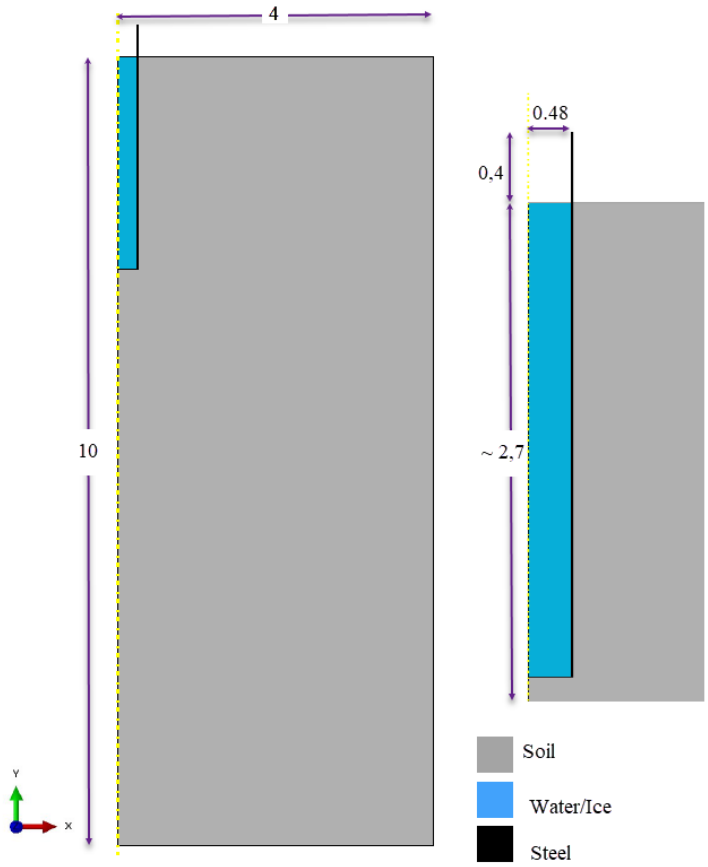

Figure 3.11: Overview of the steel foundation model (dimensions in m)

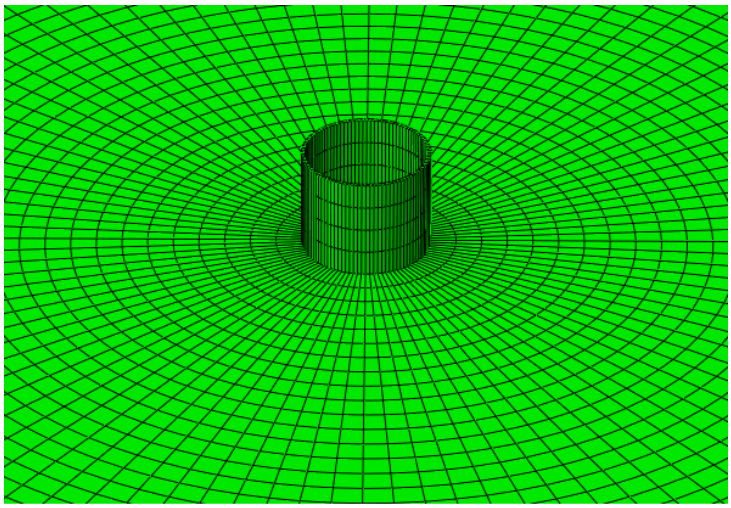

Figure 3.12: 3D view of the steel foundation FE-model

The temperature loading is applied to the top of the foundation. The water inside the pipe is modeled at the same level as the soil. This is considered a worst-case scenario. The steel foundation extends 0,4 (m) over the soil level. On top of it, the lattice steel

tower is mounted, hence water can only come inside of the foundation from the bottom end as a result of the groundwater.

To ensure that the FA-model is producing accurate results, a mesh convergence study was done by checking the maximum and minimum temperature value with different mesh density. For each mesh density, the temperature is recorded at the last step and presented in table 3.12.

Table 3.12: Mesh convergence check

Mesh density		T_{min}	T_{max}
Element size (m)	Number of elements	(°C)	(°C)
0,30	463	-0,03	1,69
0,21	962	-0,08	1,70
0,15	1879	-0,17	1,71
0,10	4004	-0,30	1,71
0,07	8242	-0,32	1,71
0,05	16208	-0,35	1,71

By using the data from 3.12, a graphical representation is given in figure 3.13. Figure 3.13 shows how the minimum and maximum temperature changes by increasing the number of elements in the model.

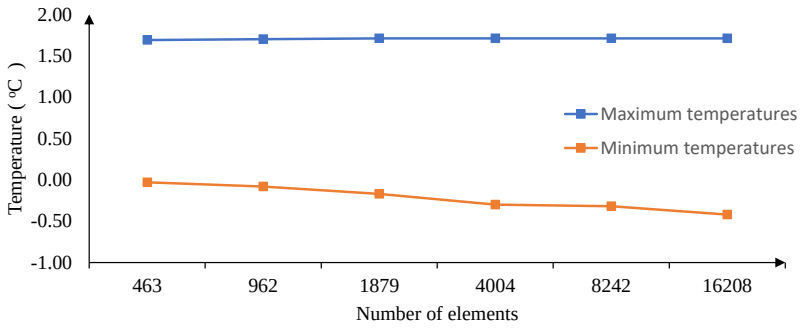

Figure 3.13: Diagram of the mesh convergence check

For the mesh density test, the boundary conditions, geometry, and all the other parameters are kept the same as in the primary model. The only difference is that the temperature is applied over a period of 30 days only. The main simulation will be run with a temperature applied over 760 days, as described in section 3.3.1.6

Since the temperature is applied on the top surface, as a result, deeper, we check less sudden changes can occur in temperature because of the distance the heat has to travel;

hence the temperature is more stable. See the plot for maximum temperature from figure 3.13.

Closer to the surface, the temperature fluctuates more, resulting in a less accurate value when using a coarser mesh. By increasing the mesh density, pass 1879 elements, the minimum temperature values begin to stabilize. The mesh size has been set to 100x100 (mm), resulting in 4004 total number of elements, which has been found to be a good balance between computational cost and accuracy.

3.3.3 Results and discussion

The first analysis was run based on the surface temperature plotted in figure 3.10 to evaluate the ice plug based on the temperatures recorded in the area of Alta. Figure 3.14 presents the temperature profile at the foundation center line at various times.

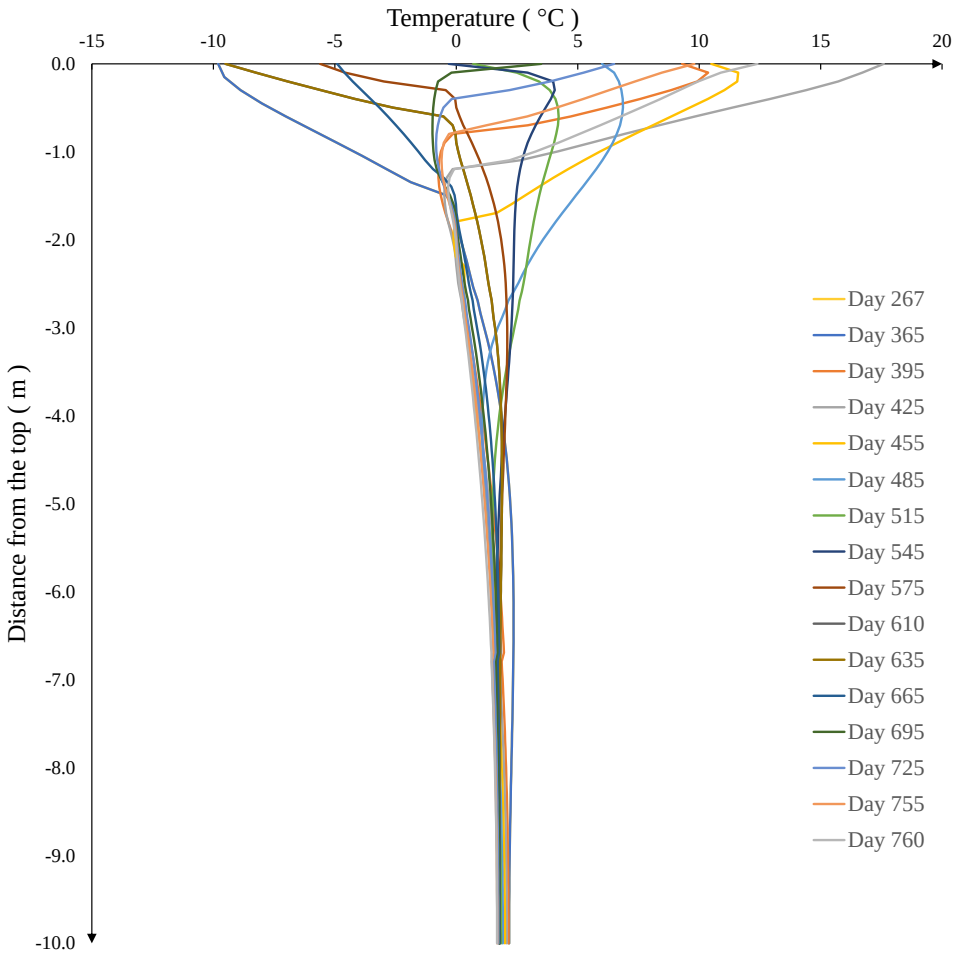

Figure 3.14: Scenario 1: temperature profiles at different times for Alta

It can be observed from the plot in figure 3.14 how temperature varies between negative degrees and positive degrees. The variation is more frequent up to a depth of roughly two meters; after that the temperature is more stable. This was expected since closer to the surface; the effect of the change in temperature has a greater impact.

The maximum ice plug for this simulation for a fully frozen plug -1 (°C) is 1,32 (m), whereas the maximum depth to which ice is formed -0,1 (°C) is approximately 1,60 (m). The sensitivity of the temperature criteria can be seen in figure 3.15.

Notice that the frost depth next to the wall of the pipe, is higher than in the middle of the pipe. That is because of the steel's ability to conduct heat.

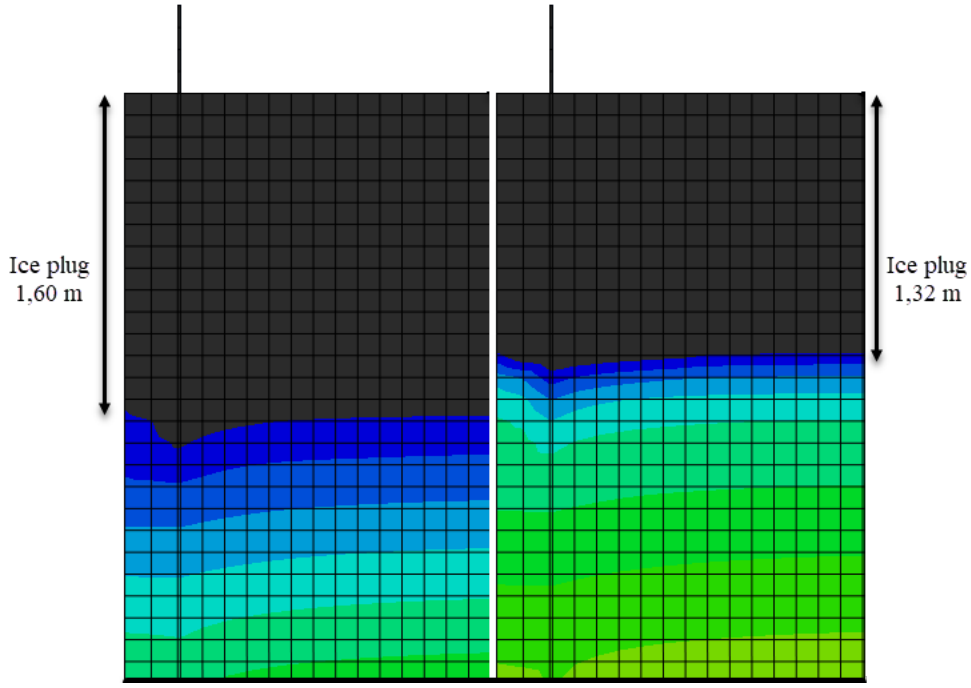

Figure 3.15: Ice plug length according to two criteria at day 635 -0,1 (°C) (left), -1 (°C) (right). The location of the steel pipe and foundation is shown in black.

Figure 3.16 shows the formation of two ice plugs, a thin one on top and a larger one further down. Two ice plugs can occur if the ice in the foundation melts partly from the top prior to a second freeze period. When this happens, water is trapped between the two plugs, if a new freezing period occurs, the water between the plugs will freeze, and so applying pressure on the wall of the pipe and on the existing ice plugs. However, the thermal analysis shows that the top ice plug is melting the next day; hence no water is trapped.

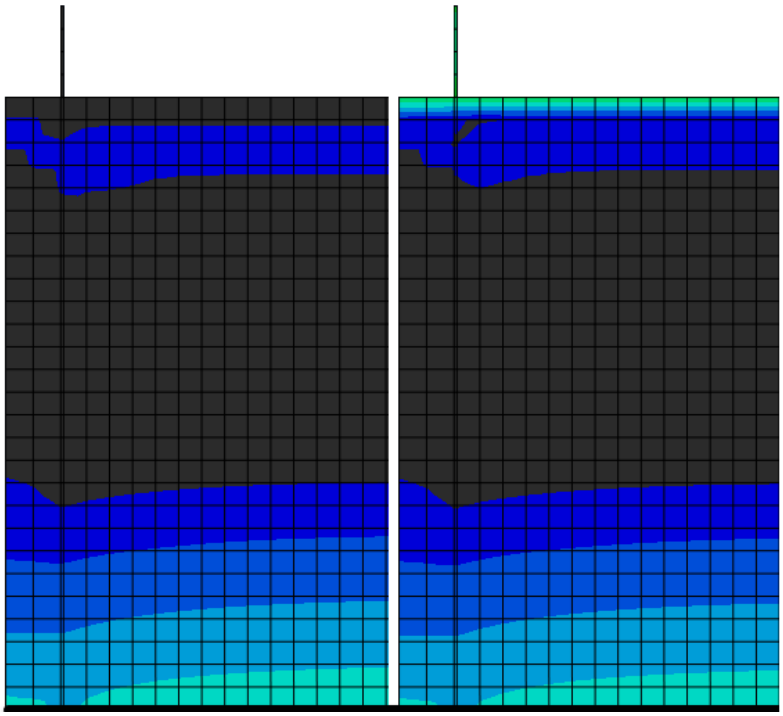

Figure 3.16: Two ice plugs occurrence at day 680 (left), top ice plug melted at day 681 (right). Ice is coloured in grey, water is blue

Based on the meteorological institute's temperature profile, the two plugs scenario that occurred is not considered dangerous for the steel foundation. However, it is possible that a temperature profile that leads to more durable ice plugs can occur. To further investigate this scenario a new temperature profile is created, see figure 3.17.

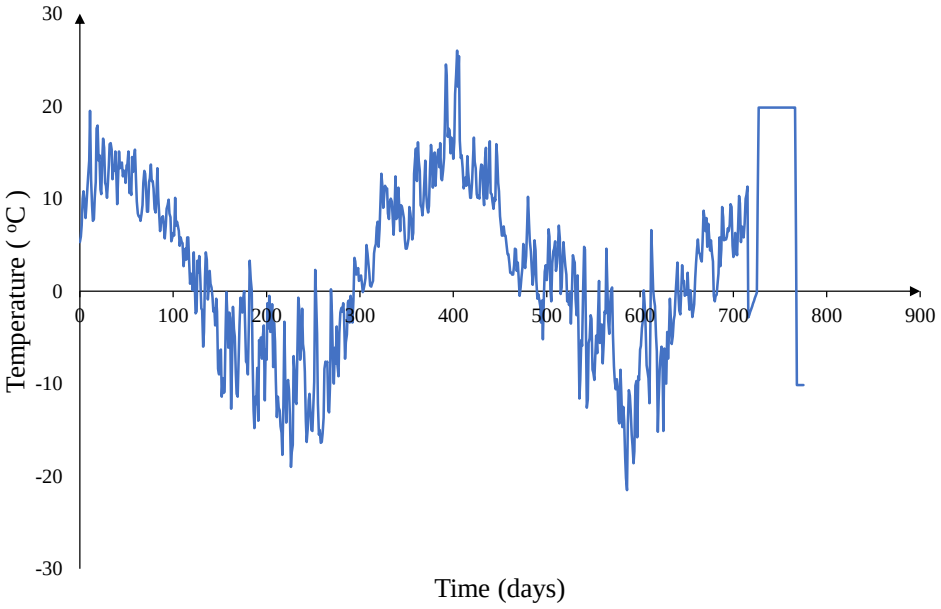

Figure 3.17: Average day temperature in Alta, followed by extreme heat and cold periods

The diagram shows a prolonged heat period at 20 (°C) defined at the end of the second winter period, followed by a new cold period at -10 (°C). The heat and cold periods are extreme and are assumed to be unlikely to occur.

Even so, the size of the ice plugs formed as a result of the extreme temperatures gives an indication of a worst-case scenario and what it could mean for the foundation.

Figure 3.18 shows the results of the simulation. Two ice plugs are formed. On the top, the ice plug measures approximately 0,5 (m), and the bottom of the plug is 1,6 (m).

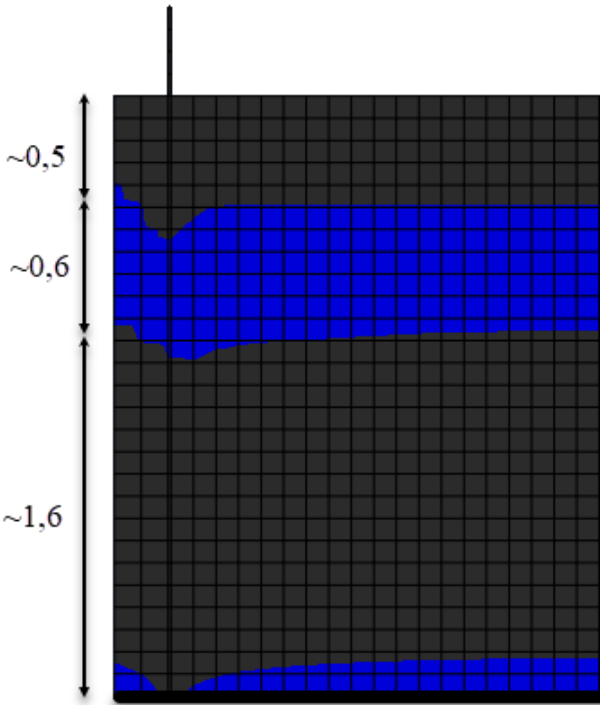

Figure 3.18: Two ice plugs as a result of extreme heat and cold periods

The plot given in figure 3.19 shows how temperature changes with the distance for the two ice plugs simulation. The top plug is strongly affected by the temperature up to approximately 0,5 m depth, after which the water is getting supercooled but yet is not freezing. If the temperature keeps decreasing, the confined water will begin to expand.

The structural effect the formation of two plugs has on the foundation will be discussed in a later chapter.

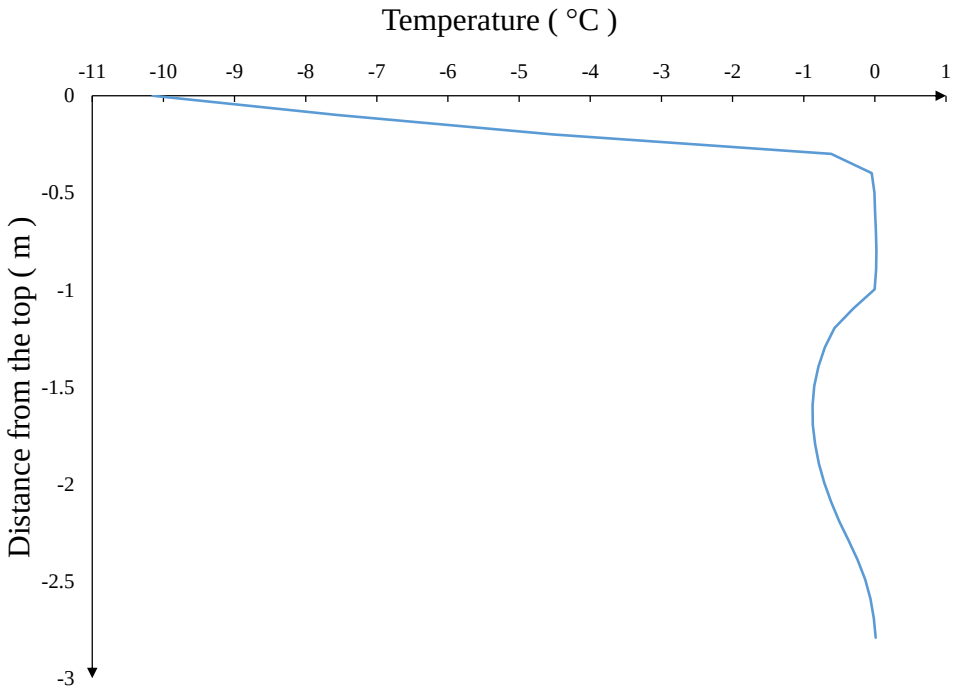

Figure 3.19: Temperature plot for the two plugs scenario

With the methodology used, where latent heat is implemented with a non-linear heat capacity, it is not so easy to define a temperature criterion for the two-plug scenario. A plug is considered fully formed at -1 (°C) and fully melted at 0 (°C). For the model to represent two ice plugs, one at the bottom due to partial melting and one freezing from the top, the temperature limit was set to -0.5 (°C). This is considered to give a rough estimate of the size of the two ice plugs.

For the second scenario where the surface temperature was changed with the one that defines a 100 – years return period, as expected the size of the ice plugs has increased.

The maximum ice plug for a fully frozen ice plug has been found to be 1,95 (m), while the maximum depth at where the ice started to form is 2,39 (m). See figure 3.20 below. The temperature profiles for various dates are plotted and given in figure 3.21.

This simulation gives the worst-case scenario, while the first analysis is assumed to be a more realistic representation while keeping in mind that it is only based on the lowest temperatures recorded in the last ten years.

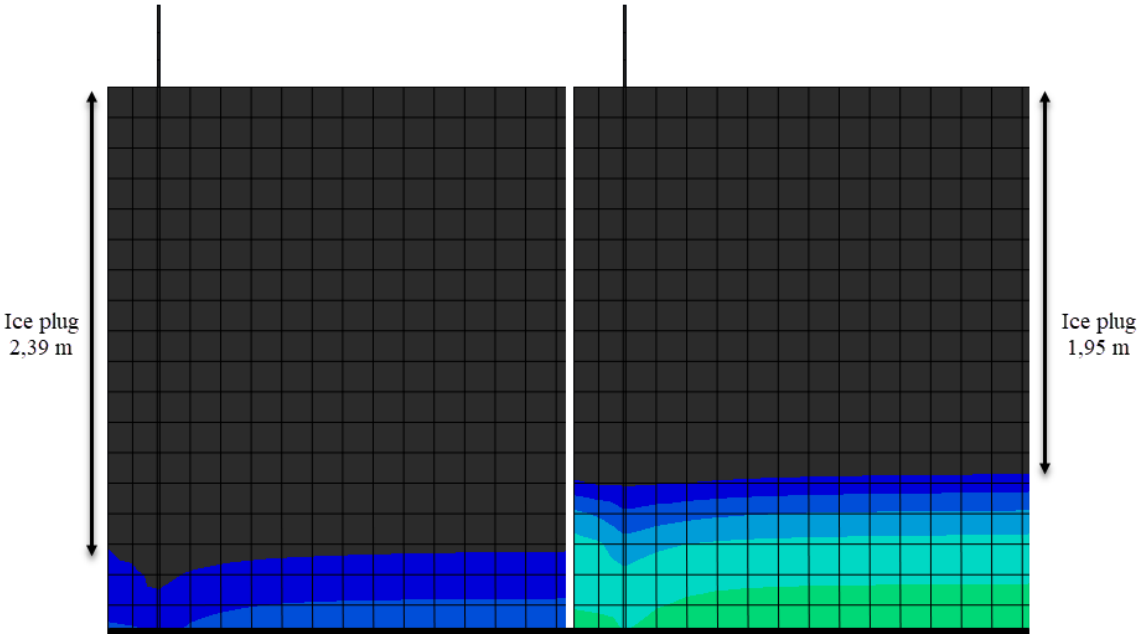

Figure 3.20: Ice plug length according to two criteria at day 709 -0,1(°C) (left), -1(°C) (right). The location of the steel pipe and foundation is shown in black.

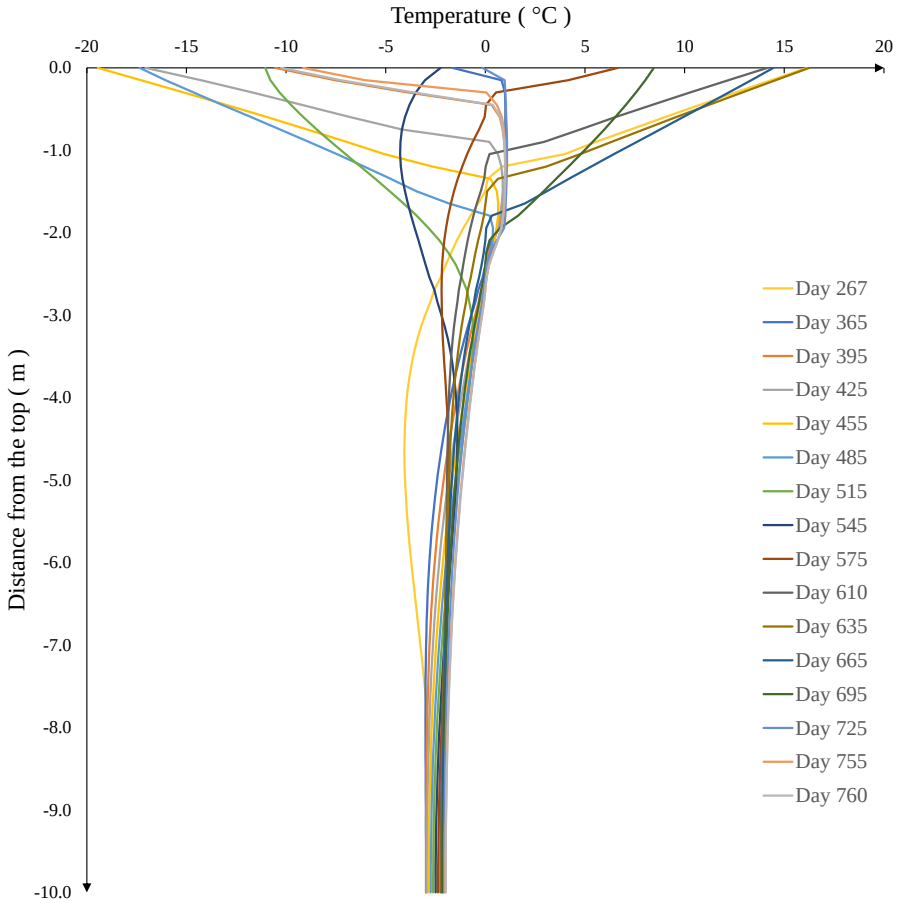

Figure 3.21: Scenario 2: Temperature profiles at different times for Alta, 100-year return period

The conservative simulation gives a more considerable value of the ice plug mainly because it assumes a sinus curve with temperature fluctuating over a very long time period. The temperature begins to decrease, and it stays negative for a long period. As a result, the ice plug keeps increasing until the warmer period starts again.

On the other hand, in the area of Alta, it is not unusual for the temperature to vary from minus degrees to positive degrees in the course of 48 hours especially at the end of the winter. Having a few days in the winter period with positive degrees can have a significant effect on reducing the size of the ice plug, which is exactly what we see happening in the first simulation.

A summary of the result is presented in table 3.13 below.

Table 3.13: Summary of the results

Scenario	Plug (m) at T:	
	-0,1 (°C)	-1 (°C)
Realistic	1,6	1,32
Conservative	2,39	1,95

Note that the realistic scenario refers to the simulation where the input temperature is based on the daily average temperature recorded in Alta, figure 3.10. The conservative scenario is based on a 100-year return period, figure 3.6.

3.3.3.1 Sensitivity of the parameters

The input soil parameters in the analysis were based on typical values for frost-susceptible soils given by Byggforsk (Byggforskserien, 2018). However, the properties of the soil may vary, especially the density. Different soil density can have different water content. If the density and water content change, so does the latent heat.

Soil samples from other projects done by Statnett in the South of Norway have shown that a density of 1900 (kg/m^3) and water a content between 12-15% are not uncommon. The density and water content vary slightly in comparison with Byggforsk's recommendation. Regardless, a simulation was performed to investigate how the ice plug changes, see table 3.14. The simulation was run with the temperature profile for a 100-year return period (the conservative scenario).

Table 3.14: Simulation results with alternative density parameter

Return period	Plug (m) at T:	
	-0.1 (°C)	-1 (°C)
100-year	2,84	2,40

By changing the density and water content, the ice plug's size increased with approximately 0, 4 (m). The main reason is because of the latent heat of the soil. When water freezes, it releases energy in the form of latent heat. A higher value of dry density and a smaller value of water content give a lower latent heat value. The latent heat, when released, acts as a brake by increasing the temperature and slowing down the cold. Hence a lower latent heat value, less energy is released; therefore, deeper in the soil, the ice front moves.

The analysis shows that the depth of the ice front is strongly dependent on the density and water content. However, for the foundation to be filled with water, soil with high water content is required. The investigation of the thesis assumes a worst-case scenario when the pipe of the foundation is filled with water. Therefore, when the pipe in not filled with water up to the ground level, the situation is considered less critical for the foundation.

4 Theory of material behavior

This chapter covers the properties of ice and the process of water freezing, followed by the mechanism that can be damaging for tubular sections when water is freezing inside. Furthermore, the theory required for analyzing the strength capacity of the tubular part of the foundation is presented. When water freezes, the volume expands by approximately 9%. The value of the force exerted by water as it freezes is dependent on several factors including the temperature, pressure and the material in which it freezes. The pressure exerted by freezing water has through history caused a number of damage to structures and structural elements. Some examples here are the bursting of pipes, the crush of the hulls of ships trapped in ice and the offset of foundations and buildings. The forces that water creates when it freezes can be extremely high and, in theory, based on the phase diagram of ice a value of approximately 200 MPa can be read, assuming the water freezes in an infinitely stiff container (Akyurt et al., 2002).

4.1 Properties of ice

To fully understand the mechanism that breaks pipes, a brief study of the freezing process and properties of ice are undergone in this chapter. In tubular sections at low temperature when water changes states from liquid to solid it expands; this expansion leads to stresses which are acting on the walls of the tube. As mentioned previously the density of water is dependent on temperature.

Water is most dense at 4 (°C), after which the density decreases with the temperature. This behavior of water is the reason why ice floats for example. Ice can exist in different forms; the way ice forms is dependent on pressure and temperature. The phase diagram in figure 4.1 shows the different types of ice structures at different temperatures and pressures. In figure 4.1 the horizontal axis is temperature given in degrees Celsius and the vertical axis is the pressure expressed in MPa. All-natural ice found on earth is of the type Ih and has a hexagonal dendritic form. The Ih ice type it can be seen from the diagram is stable between 0 (°C) to -200 (°C) and up to a pressure of 200 (MPa). Other types of ice structures are shown in the diagram II, III, etc. For most common engineering problems the Ih ice type is encountered (Akyurt et al., 2002).

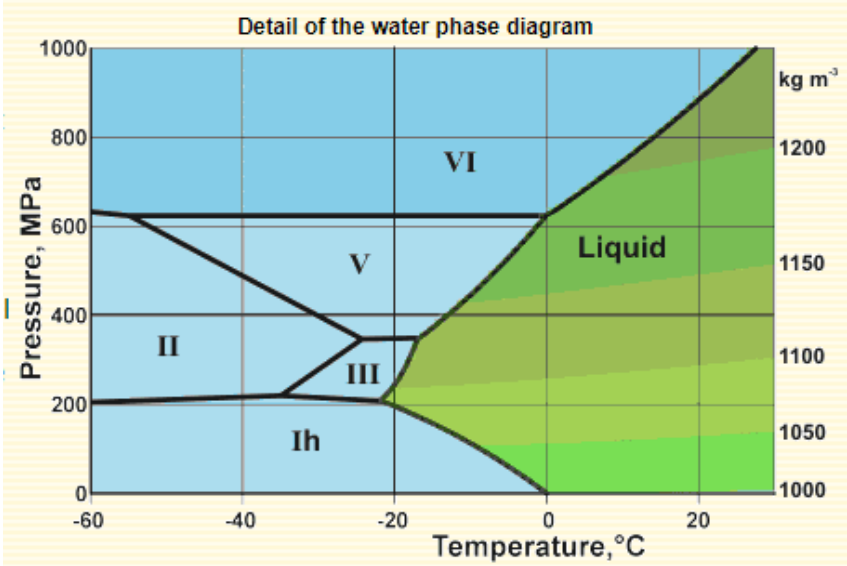

Figure 4.1: Water phase diagram

4.2 Mechanical behavior of ice

The same as other solids ice Ih exhibits three stages when an external force is applied: elastic, plastic and a brittle stage. The elastic behavior is anisotropic, and the young's modulus varies by less than 30% between the loading direction for a single ice crystal. In general, for ice, the young's modulus is dependable on the purity of ice, temperature, frequency of stress, the time of applied stress and several other factors. Figure 5.2 below shows the stress-strain curves for ice at different strain rates: low (I), intermediate (II), and high (III). From the diagram it can be seen for both tension and compression at a low strain rate (I) that the behavior of ice is ductile. In tension, at intermediate strain rate, the ice displays a brittle behavior because the applied load leads to initiation of cracks while in compression the behavior stays ductile. Further regardless of tension or compression at a high strain rate, the behavior of ice is brittle (Schulson, 1999).

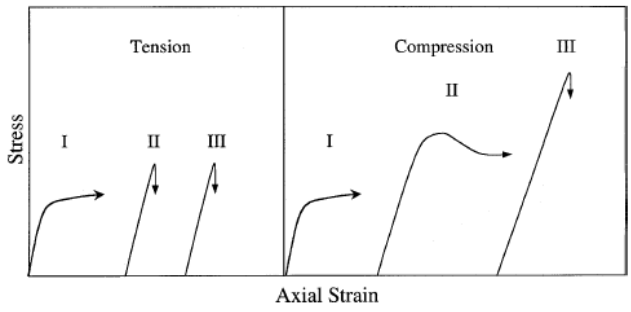

Figure 4.2: Stress-strain curves for ice (Schulson, 1999)

Even though the elastic modulus and the yield strength of ice are dependent on several factors mentioned earlier, it has been shown that the factor of utmost importance for both the elastic modulus and the yield strength is in fact the strain rate. By knowing the strain rate, it is possible to approximate the yield strength of a given type on ice by reading it from figure 4.3 below.

The diagram in figure 4.3 shows the compressive strength of different types of freshwater ice at various strain rates. Freshwater ice is the ice that is formed from lakes, rivers, and groundwater. Further freshwater ice in the diagram is divided into T1- granular ice, S1- columnar large crystals ice, S2- smaller crystal ice, and S4- frazil ice (Gold, 1977).

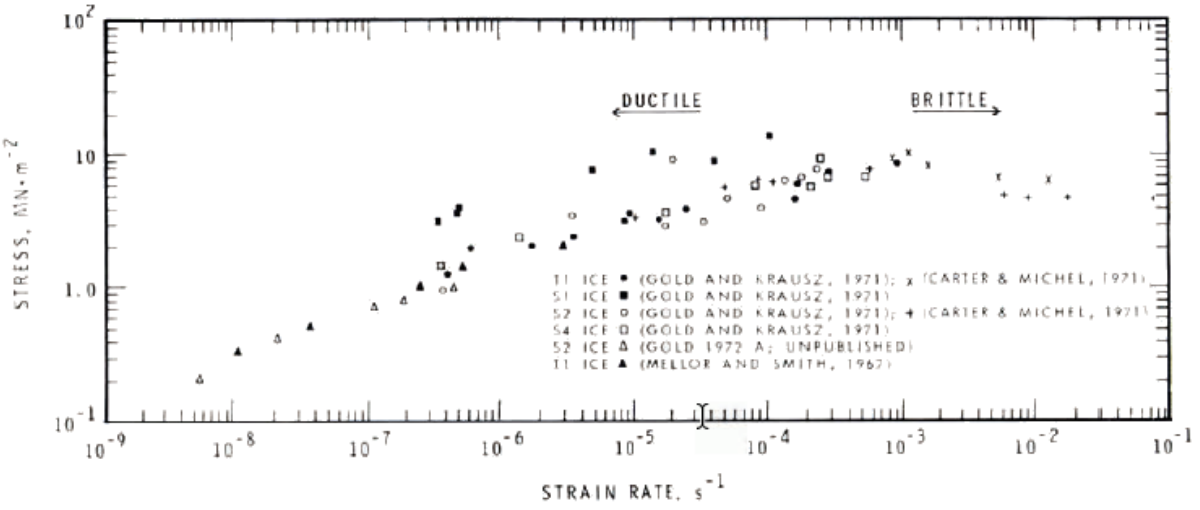

Figure 4.3: Yield and brittle strength dependence of strain rate (Gold, 1977)

Another property of ice that is very important for the mechanism that leads to structural failure in steel tubes is the adhesion of ice. The damage done by ice adhered to structures every year is very costly, a few examples here are damage done at road surfaces, high voltage cables, airplane wings and so forth. Adhesion of ice can be defined as the ability of ice to cling to other surfaces. Experiments have been conducted to measure the adhesion strength of ice on different materials. Different materials have different adhesion mechanisms to ice, and the strength of adhesion is also dependent on several factors. Some of the factors are surface pattern, temperature and the ice's microscopic structure. When it comes to the adhesion strength of ice on steel surfaces, experiments have shown a maximum strength of approximately 0,5 (MPa) in shear.

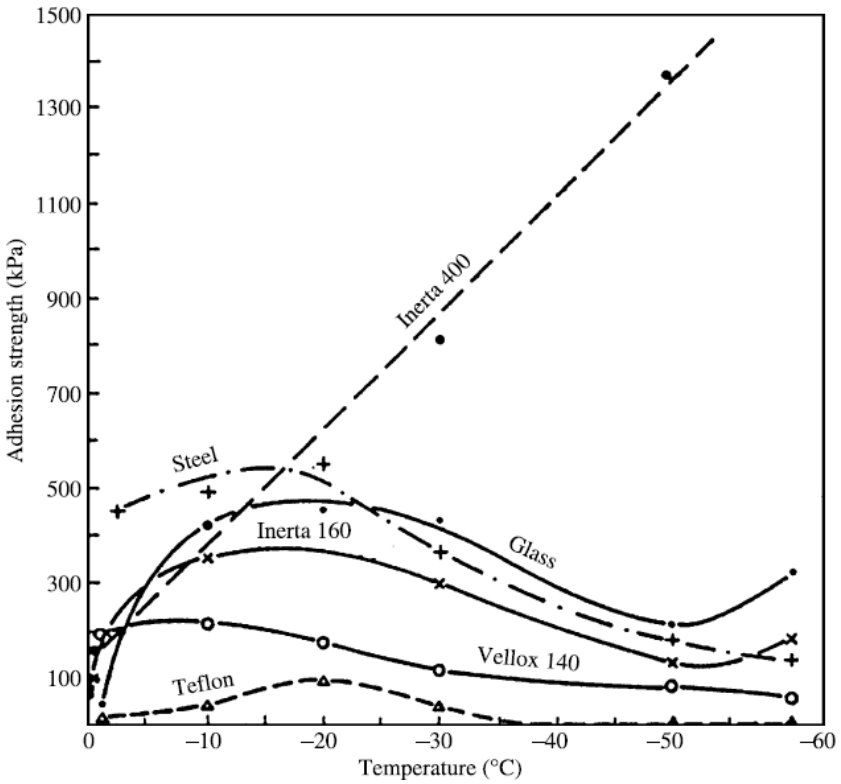

Figure 4.4: Adhesion strength of ice on different surfaces (Makkonen, 2012)

Figure 4.4 shows the strength of ice adhesion for different surfaces. Notice that for steel the highest adhesion strength is between -10 and -15 (°C). The other curves show the adhesion strength of ice for coated surfaces. Vellox 140, for example, is an anti-icing coating, making the surface smoother hence the ice can be removed with less effort (Makkonen, 2012).

Thermal expansion of ice

In general, when a solid is exposed to high temperatures, it expands, and when it is exposed to low temperatures, it shrinks. As stated previously water is doing the opposite. When it is exposed to subzero temperatures is expanding by approximately 9 %. Further, when water becomes ice, it starts behaving similarly to a typical solid. Research shows that if ice is kept exposed to prolonged freezing temperatures, ice is shrinking. Experimental observations have been made on ice floating on rivers, lakes, and sea. When thin floating ice is suddenly exposed to very low temperatures, the ice begins to contract, and if the temperature is sudden enough, it cracks. The cracks can again be filled with water, and as a result, the ice surface keeps increasing. If, after a prolonged period with subfreezing temperatures, a period with warmer temperatures fallows, the ice is warmed up and begins to expand. Further, if an object restricts the expansion, thermal ice pressure is created.

Thermal ice pressure can be critical for structures that are built next to the shores, for example (Fransson, 1988). But not only, thermal ice pressure can also occur when ice is confined like in the case of the steel foundation. Thermal expansion of ice in general is a load case that has to be considered when designing for example offshore wind turbines (TC88-MT, 2005). In the next chapter the thermal ice pressure on the foundation will be investigated.

4.3 The freezing process in tubular sections

For water, when the temperature drops below 0 (°C) the phase transition from liquid to solid begins. For a tubular section filled with water when exposed to subfreezing temperature from all directions the freezing process can be divided into four stages:

1. Cooling
2. Dendritic ice formation
3. Annular ice formation
4. Final cooling

In the first stage when the pipe is exposed to the subfreezing temperature the water temperature drops. The heat transfer mechanism from water to the ambient is by convection and conduction. According to experiments, the water in the pipe does not immediately begin to freeze when the temperature of 0 (°C) is reached but continues to fall until the water temperature reaches the ambient temperature. This process is also referred to as supercooling. In the second stage the dendritic ice forms. The formation of ice leads to the release of latent heat which raises the temperature of the water. Hence a spike in temperature can be seen in various experiments. After the formation of dendritic ice is done in stage three annular ice begins to form. The annular ice is a denser type of ice. In this stage, the dendritic ice from the second stage is embedded in the annular ice. The final stage referred to as final cooling is when all water is transformed into solid annular ice. All stages are illustrated in figure 4.5 below (Gordon, 1996).

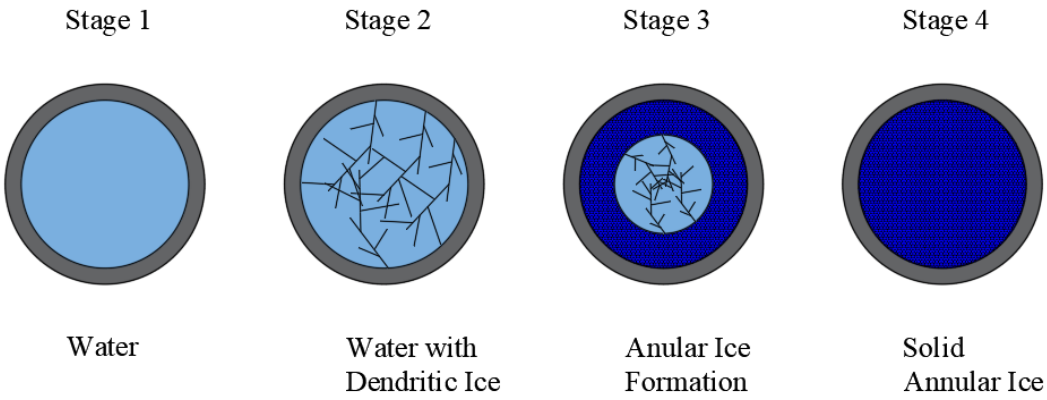

Figure 4.5: Freezing process in a tubular section (Gordon, 1996)

4.4 Freezing scenarios in vertical tubular sections

Previously the process of freezing and the stages water goes through before it becomes solid ice has been presented. To understand the impact water has when it freezes on the steel foundation an assessment of different freezing scenarios is analyzed. It is a common misconception that tubular sections are being damaged when ice growth pushes against the walls of the tubular section.

Research has shown that in fact bursting of pipes happens when a solid plug of annular ice is formed inside a pipe, and it pushes the remaining water in a confined space leading to increase pressure on the walls of the pipe. In other words, it is not the ice growth that damages the pipe but the trapped water in a confined volume. It is also important to mention that dendritic ice formation can't lead to a pressure build high enough to rupture the pipe, only when ice has entered stage 4, solid annular ice the rupture can occur. When the pressure of the confined water is high enough the wall of the pipe will begin to fracture creating a crack and the release of the pressure by forcing the water out (Akyurt et al., 2002).

The pipe orientation and the surface/surfaces from where the ice begins to form plays a significant role in the pressure build. Below different scenarios for the freezing mechanism in a vertical tube section are presented and explained. For all the scenarios presented below, assumed a vertical tubular section closed at the bottom end and open at the top end is assumed.

As mentioned previously the steel foundation which is the topic of this master thesis

consists of a tubular steel section mounted vertically on top of a steel pad. By analyzing the different cases below a conclusion of what happens to the steel foundation when water freezes can be formulated. The following five cases of ice expansion have been identified:

1. Water freezes from the bottom and up

2. Water freezes from the walls

3. Water freezes from the top end

4. Water freezing from bottom and top-end

5. Water freezes from all sides

Case 1: Water freezes from the bottom and up

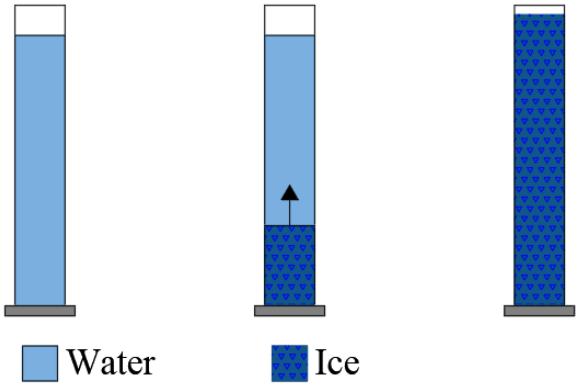

Figure 4.6: Freezing from the bottom end

In this case, the water starts freezing from the bottom only, it is assumed that all other surfaces are fully insulated. The ice will grow faster along the cylinder walls, as the thermal conductivity of steel is higher than that of ice. The expansion of ice is pressing the water up, where water can escape freely. As a result, there will be no pressure build-up in this case.

Case 2: Water freezes from the walls

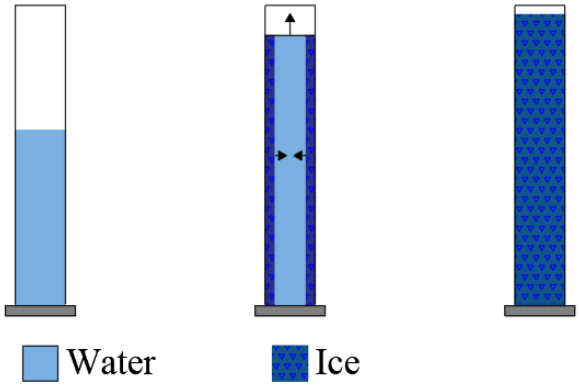

Figure 4.7: Freezing from the walls

For the second case, the water is freezing from the walls and inwards. The same as in the previous case it is assumed that all other surfaces are insulated. As long as water freezes with the same velocity from both sides there will always be a gap in the middle where water can freely expand. In this case, they will be no pressure build, hence the tubular section will not be damaged because of the water freezing.

Case 3: Water freezes from the top end

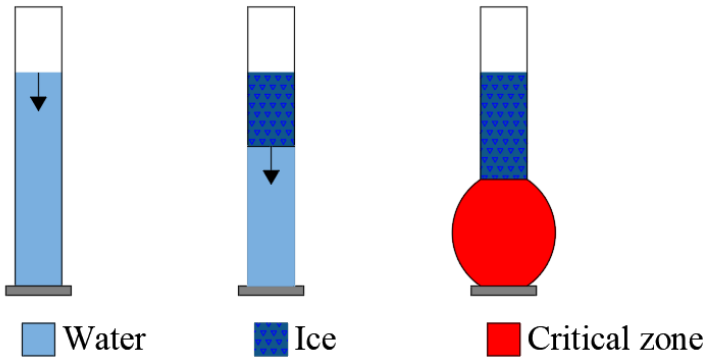

Figure 4.8: Freezing from the top

This scenario is critical for the tubular section and is directly related to the theory discussed earlier. When water freezes from the top the expansion of ice is driving the water into a confined space. As a result, the pressure will keep increasing until the pipe ruptures, allowing some of the water to be released. It is important to note that the rupture of the pipe is dependent on several factors, including the material of the pipe, freezing temperature, and the dimensions of the pipe. In some cases, the expansion of

ice may only create a high stress on the walls of the pipe and not rupture it or deform it. This case can be critical for tubular sections.

Case 4: Water freezing from bottom and top-end

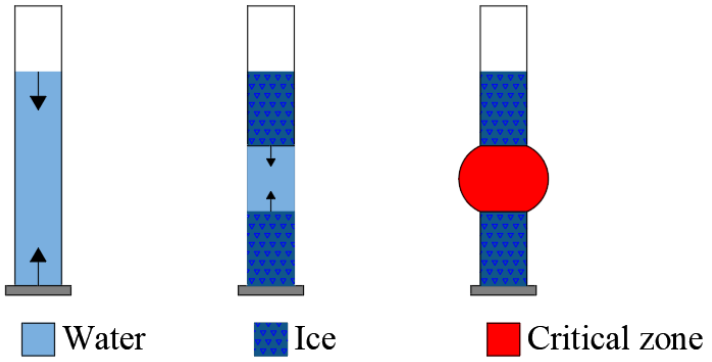

Figure 4.9: Freezing from the bottom and from the top

This is another critical scenario for a tubular section. In this case, water is freezing from both ends leading to the formation of two ice plugs that will keep growing trapping the water between them. The confined water leads to a pressure build creating a critical point in the middle of the section.

Case 5: Water is freezing from all sides

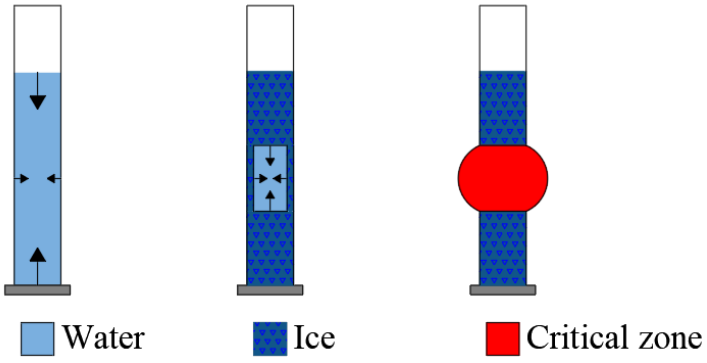

Figure 4.10: Freezing from all sides

This is a combination of all the cases presented above. For this to happen the tubular section must be exposed to freezing temperatures from all sides. When ice is expanding from all sides water is trapped somewhere in the middle, resulting in a pressure build that can be critical for the pipe.

4.5 Thin walled pressure vessel

A thin walled pressure vessel is one in which the walls have a thickness that is much smaller than the overall size of the vessel, and the vessel is subjected to internal pressure that is much greater that the exterior air pressure. In order for a vessel to be categorized as thin walled the following expression must be met (Ibrahim et al., 2015):

$$t < \frac{r_m}{10} \tag{4.1}$$

where:

t is the wall thickness

r_m is the middle radius

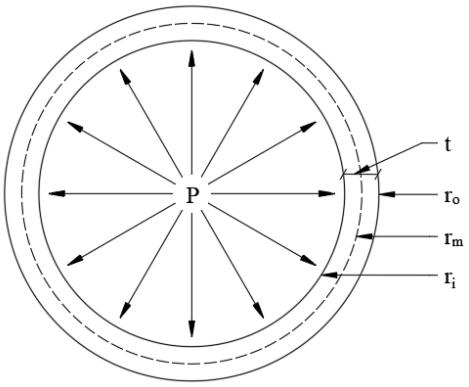

Figure 4.11: Section of the pipe showing the internal pressure, radiuses and the wall thickness

When an internal pressure P is acting on the walls of the vessel to satisfy equilibrium there must be some forces which counteract the internal pressure P.
The counteracting force in the longitudinal direction is called the axial stress or the longitudinal stress and is given by the following equation (Ibrahim et al., 2015):

$$\sigma_a = \frac{Pr_m}{2t} \tag{4.2}$$

where:

σ_a is the axial stress

P is the internal pressure

r_m is the middle radius

t is the wall thickness

Further the second stress counter acting the internal pressure P is called the tangential or the Hoop stress and is given by the following equation (Ibrahim et al., 2015):

$$\sigma_t = \frac{Pr_m}{t} \tag{4.3}$$

where:

σ_t is the axial stress

P is the internal pressure

r_m is the middle radius

t is the wall thickness

4.6 Yield criterion

A yield criterion defines the the limit of elasticity in a material and the onset of plastic deformation under any possible combination of stresses. There are a few yield criteria. For metals, the von Mises Yield Criterion is most often used. According to the criterion, yield occurs when the von Misses stress is equal or greater than the yield strength σ_Y divided by a material factor. The yield strength σ_Y is usually determined in a uniaxial tensile test (Irgens, 2006).

$$\sigma_{VM} \leq \frac{\sigma_Y}{\gamma_{M0}} \tag{4.4}$$

Von Mises stress criterion is defined as:

$$\sigma_{VM} = \sqrt{\frac{1}{2}[(\sigma_1 - \sigma_2)^2 + (\sigma_1 - \sigma_3)^2 + (\sigma_2 - \sigma_3)^2]} \tag{4.5}$$

For a two-dimensional plane stress state, the von Mises stress can be defined as:

$$\sigma_{VM} = \sqrt{\sigma_1^2 - \sigma_1\sigma_2 + \sigma_2^2} \tag{4.6}$$

where:

σ_{VM} is the von Mises stress

σ_Y is the yield strength

σ_1, σ_2 and σ_3 are principal stresses .

γ_{M0} is the material safety factor

5 Structural analysis

Based on the thermal analysis, the amount of water that can freeze inside the tubular section of the steel foundation is known. This chapter will assess the structural impact ice has on the steel foundation. Based on theory from the previous chapter, three cases are analyzed below, one when water freezes from the top a second case when the thermal ice pressure is investigated and a third when temperature fluctuation leads to the formation of two ice plugs.

Summary of the cases investigated below:

- Case 1: Freezing from the top
- Case 2: Thermal expansion of ice
- Case 3: Formation of two ice plugs

5.1 Case 1: Freezing from the top

Based on the thermal analysis it has been found that the size of the ice plug can be up to approximately 2,4 (m). When the air temperature drops below 0 (°C) ice starts to form from the top and then grows downwards. The ice will grow faster along the cylinder walls because the thermal conductivity of steel is higher than that of ice, thus illustrated ice shape in figure 5.1.

However, since the foundation geometry allows water to escape at the bottom end, the pressure-rise is minimized. Since entrapped water is a prerequisite for a substantial pressure build-up, this freezing process is not considered harmful for the steel foundation. Figure 5.1 presents a schematic of the steel foundation, assuming the worst case when the foundation is filled with water up to the ground level.

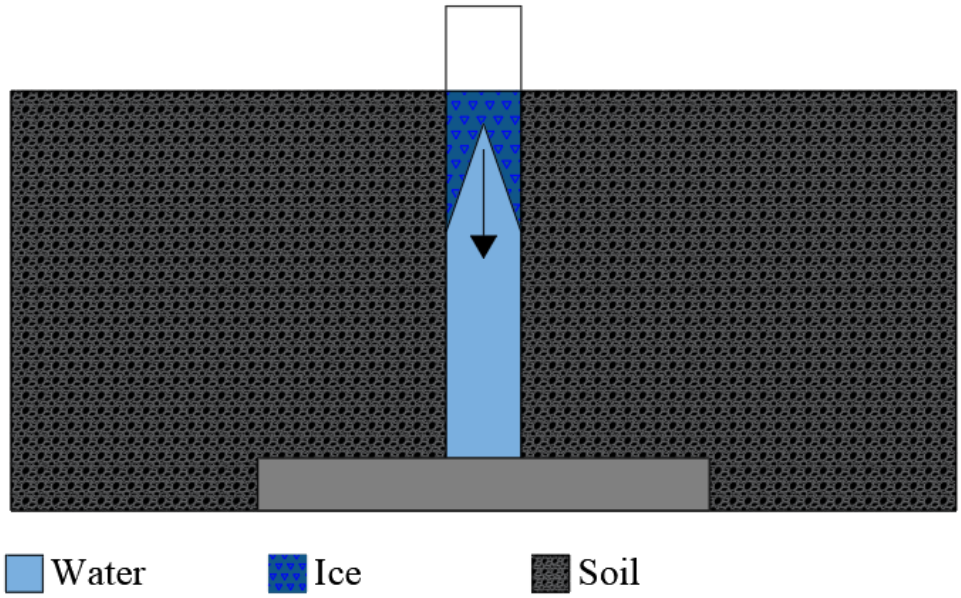

Figure 5.1: Steel foundation filled with water; freezing from the top

5.2 Case 2: Thermal expansion of ice

The theory chapter explained how ice contracts and expands when it is subjected to low temperatures followed by rising temperatures. For the steel foundation, the following case is proposed based on the theory, see figure 5.2.

Figure 5.2, illustrates the stages that lead to the thermal expansion of ice. In the first stage, subfigure *a*. an ice plug of 1,95 (m) is fully formed. The size of the ice plug was previously found from the thermal analysis.

If the temperature keeps decreasing after a period of time, the ice will begin to contract, subfigure *b*. After a period with cold temperature, warmer temperatures will likely come; as a result, the ice's top surface will start to melt and begin to fill up the space between the wall pipe and the actual ice plug, see subfigure *c*. and *d*.

If, after the warmer period, a new period will come with subfreezing temperatures, the gaps will freeze, subfigure *e*. The next time the temperature rises, ice will start to expand, applying pressure on the wall of the pipe.

The pressure that the thermal expansion of ice exerts on the pipe is further investigated in Abaqus CAE.

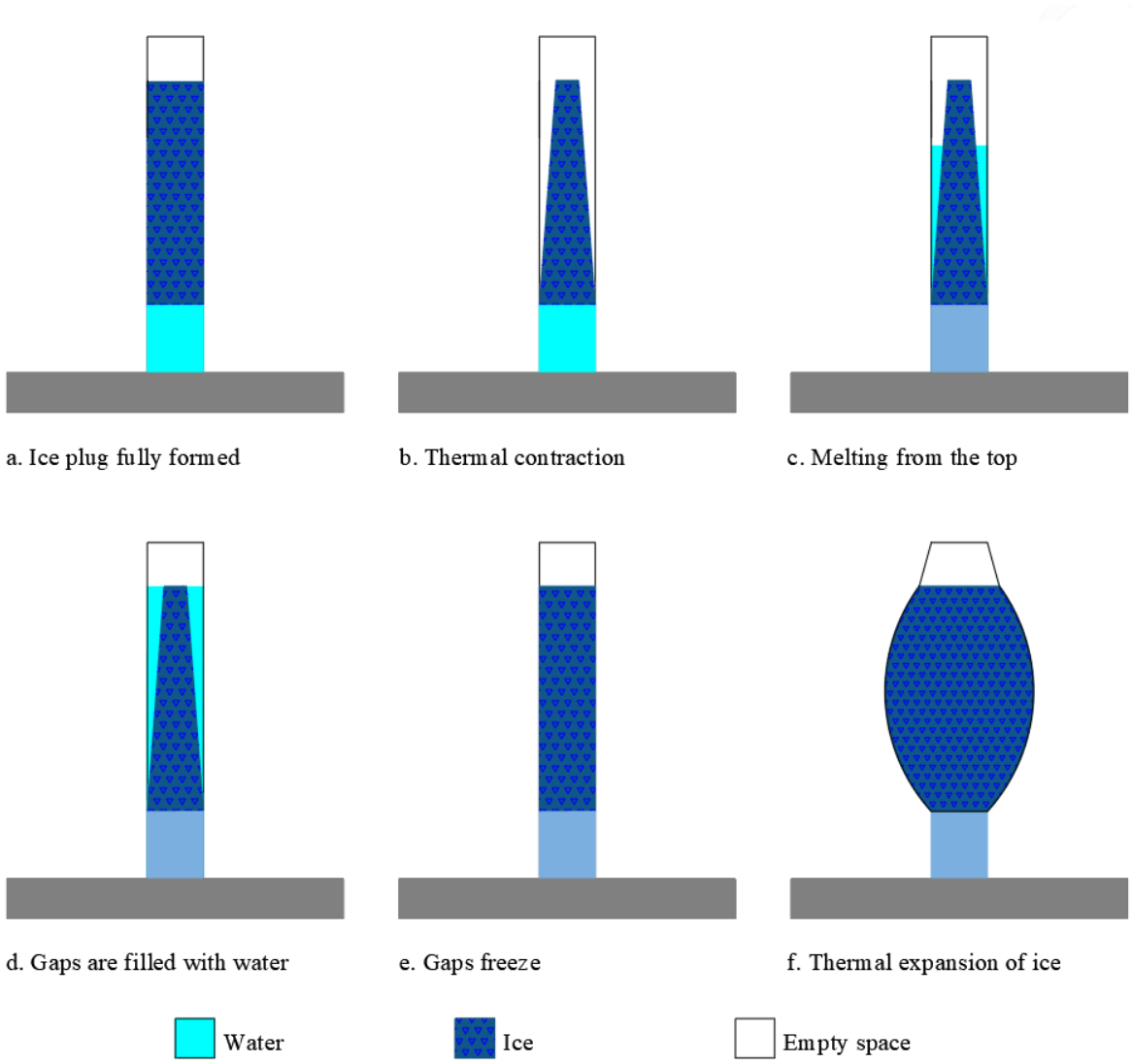

Figure 5.2: Thermal expansion of the steel foundation

5.2.1 Finite element analysis of the thermal expansion of ice

The thermal expansion of ice inside the hollow steel section of the foundation is simulated with a fully coupled thermal-displacement analysis in Abaqus CAE. A coupled thermal-displacement model is needed when the stress analysis is dependent on the temperature distribution, and the temperature distribution depends on the stress solution.

5.2.1.1 Material properties

The input parameters used in the simulation are presented in table 5.1. Most of the parameters were already discussed in the thermal analysis chapter. In addition, the young's modulus, poisson's ratio, and the expansion coefficient of both steel and ice are

added.

Table 5.1: Input parameters for the coupled thermal-stress analysis

Element type	Material properties		Units
Steel	Conductivity	60,5	(W/mK)
	Density	7850	(kg/m^3)
	Young's modulus	2,1 $\cdot 10^{11}$	(N/m^2)
	Poisson's ratio	0,3	
	Expansion Coeff.	1,2$\cdot 10^{-5}$	(1/K)
	Specific heat	434	(J/kgK)
Ice	Conductivity	2,3	(W/mK)
	Density	918,28	(kg/m^3)
	Young's modulus	9 $\cdot 10^9$	(N/m^2)
	Poisson's ratio	0,33	
	Expansion Coeff.	5$\cdot 10^{-5}$	(1/K)
	Specific heat	2048,38	(J/kgK)

The young's modulus for ice can vary considerably, as discussed previously. However, a typical average value was chosen for the simulation-based on measurements done on Ih ice type (Randhawa, 2018; Nimmo, 2004).The input parameters for steel are chosen based on the strength class of steel (Norge, 2015). The expansion coefficient for ice is based on mean values measured on samples from fresh and saline water ice (Marchenko et al., 2016).

5.2.1.2 Model setup for the analysis

The FE-model is an axis-symmetric thermally coupled that consists of two parts, steel, and ice. The model reflects the pipe geometry and the size of the ice plug found from the thermal analysis, see figure 5.3.

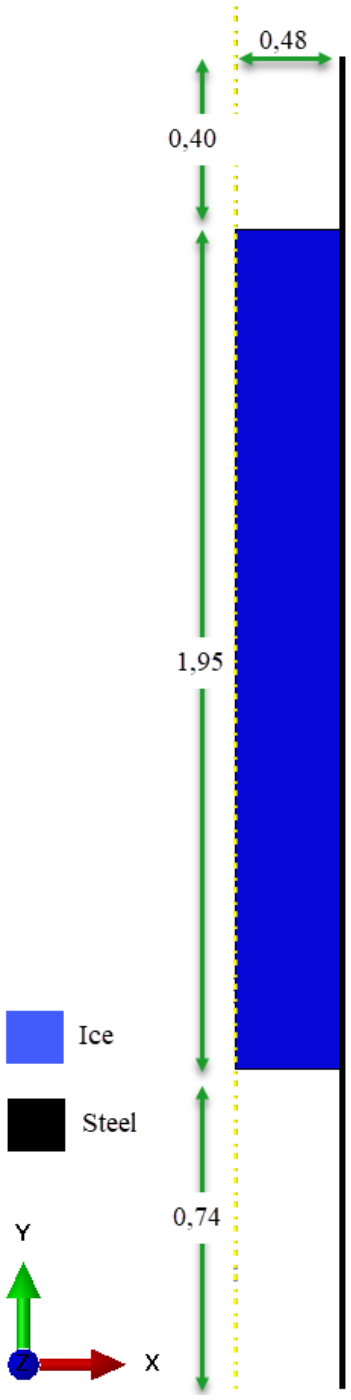

Figure 5.3: Coupled thermal-displacement model (dimensions in m)

Further, the model is given a temperature difference of 15 (°C) over a day, which is a conservative case in comparison with temperature swings from Alta, ref. the temperature plot from section 3.3.1.6. This means that the steel and the ice will expand in the course of one day. The bottom surface of the pipe is restricted in the y-direction. In reality, the pipe is mounted on the steel pad, and underneath is resting on pure soil, hence the restriction of the model in the y-direction. Since this is an axis-symmetric model the

center ax is pinned in the x-direction as well (yellow dotted line in the figure 5.3).

5.2.1.3 Results and discussion

The figure 5.7 below presents the Mises stress distribution in the model as a result of the thermal expansion. For visibility reasons, the model is divided into two parts, the figure on the left shows the upper part of the model while the one to the right gives the bottom part.

The model is meshed with 20574 elements. The mesh choice was to ensure that the thickens of the steel pipe is meshed with more than just one element. By using more than one element across the pipe thickness, the accuracy of the results is improved. It was observed by changing the mesh density; the stress value is higher than when only one element across the pipe thickens was used. This is because a higher mesh density catches is up the relatively small bending stresses as well.

Ice has a higher coefficient of thermal expansion than steel; as a result when a temperature difference is present, ice begins to expand faster than the steel, and so is applying pressure on the steel section. The highest stress concentration of approximately 110 (N/mm^2) is on the inside of the pipe wall next to both ends of the ice plug, marked in figure 5.7. The stress is highest here because of the bending stresses and the sharp angle. Further, in the middle of the pipe, an average stress value of approximately 93 (N/mm^2) is found. The stress plot along the outer side of the pipe wall is given in figure 5.4, figure 5.6 green arrow shows the path for the plot.

The plot shows higher stresses at both ends of the ice plug as expected, while the stress is more stable in the middle of the pipe. Further, in figure 5.5, the stress overtime in the middle of the tubular section is plotted. The three chart lines represent the stress overtime for the elements across the pipe thickness, denoted 1,2, and 3 in figure 5.6. The element 1 shows the highest stress since it is closest to the ice plug, followed by 2 and 3. Note that already after the first 14 hours (50400 s) the ice plug has almost reached the given input temperature and the pressure as a result of the expansion is created.

A stress value of 93 (N/mm^2) is well within the yield stress of the hollow section. Another simulation was conducted with a temperature difference of 50 (°C) over one day. The average Mises stress was found to be around 316 (N/mm^2). Based on the analysis results,

it is concluded that the thermal expansion of ice is not critical for the hollow section of the foundation. Furthermore, the stress caused by the thermal expansion is within the capacity of the steel even for the unlikely temperature difference of 50 (°C).

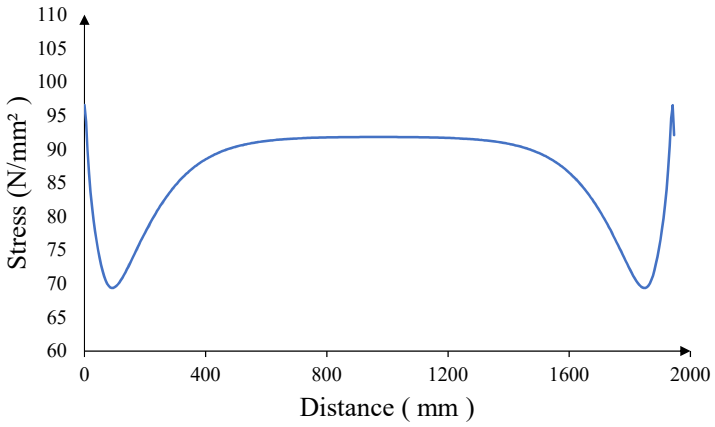

Figure 5.4: Stress distribution along the pipe's wall

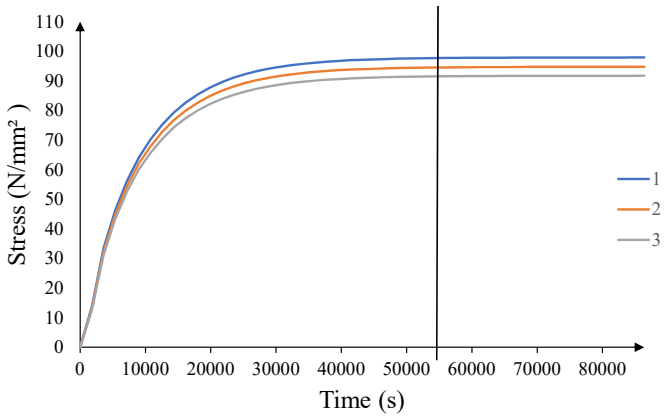

Figure 5.5: Stress distribution in the middle of the pipe

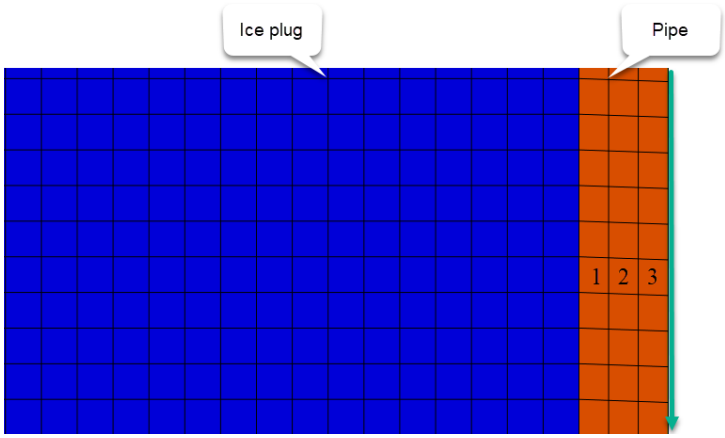

Figure 5.6: Close up view in the middle of the meshed model

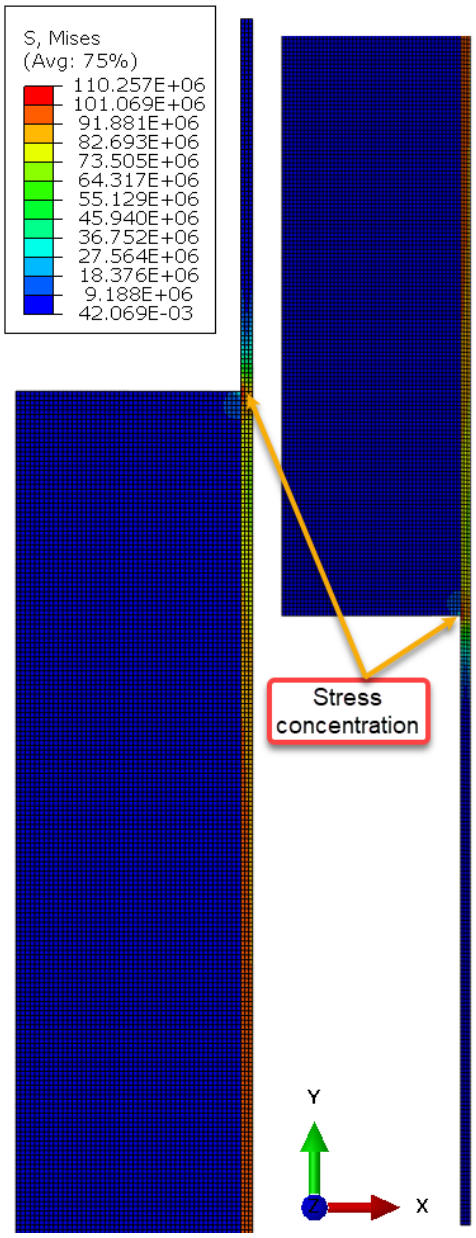

Figure 5.7: Stress contour in the model due to thermal expansion of ice (units in N/m^2)

5.3 Case 3: Formation of two ice plugs

The formation of two ice plugs can occur if an ice-filled steel foundation will melt from the top. If, after a period of melting the foundation is again exposed to a prolonged period of sub-zero temperatures, ice will form at the top and grow downwards in the vertical pipe. In this case, the water can be trapped, between the not-yet melted lower part of the ice column and the newly formed ice on the top. The phenomenon is illustrated in figure 5.8 below.

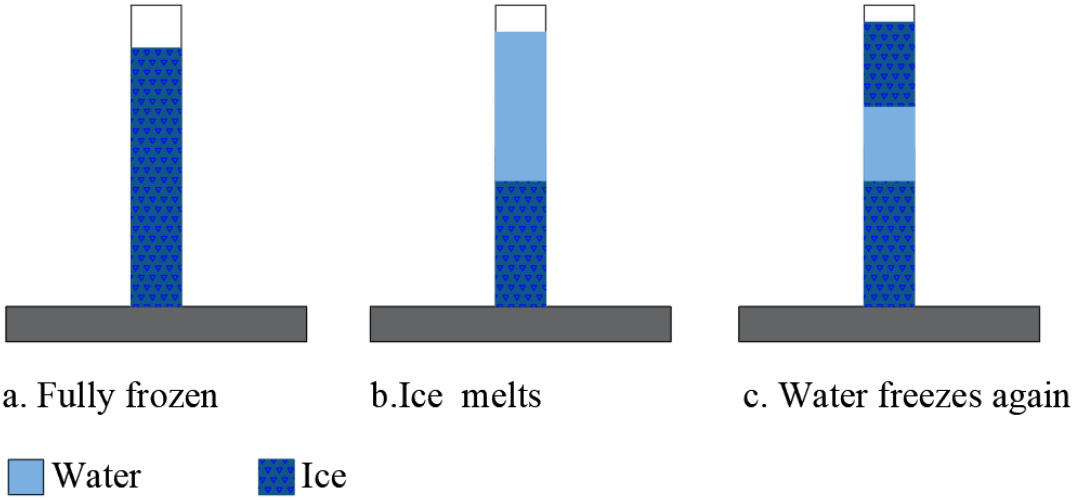

Figure 5.8: Formation of two ice plugs

However, for this scenario to be critical the following conditions must be met:

- The ice plug at the bottom and top must be large enough to support a critical pressure build-up
- An ice column of sufficient height must be formed before the melting period
- There must be enough water in the vertical pipe

The thermal analysis has shown that based on temperatures from the meteorological institute the formation of the ice plugs doesn't meet the conditions named above. Almost immediately after the ice plug on the top is formed a period with warmer temperature follows leading to the melting of the top ice plug. Hence no pressure is built up. It is possible that in the future a temperature profile that leads to the formation of two fully formed ice plugs can occur. To further investigate this phenomenon a thermal analysis was conducted with a temperature profile which induces the formation of two ice plugs, figure 3.17. Based on the results from the thermal analysis will further investigate the strength capacity of the pipe with respect to the formation of two ice plugs.

5.3.1 Analytical solution

When an internal pressure builds up between two ice plugs, the plugs are assumed to fail due to shear stresses at the ice/steel boundary. This shear stress can be found for a certain internal pressure and can be compared to the stress limit of ice. In subsection 4.2,

the maximum ice adhesion strength has been determined to have a value of 0,5 (MPa), where the yield strength (brittle if high enough strain rate) can be found from figure 4.3 if the strain rate is known.

The internal pressure that the pipe can withstand is calculated based on the theory presented previously.

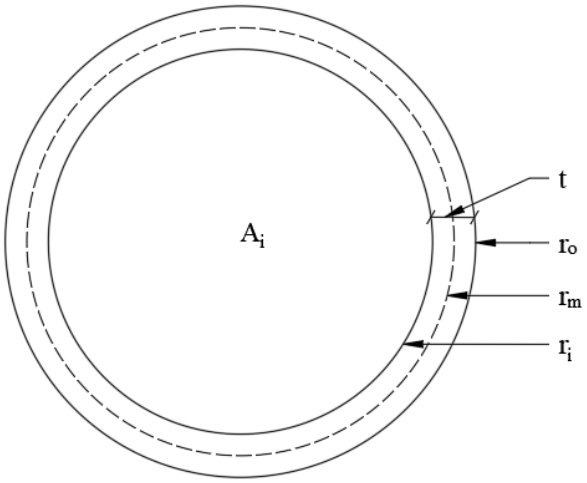

Figure 5.9: Cross section of the pipe presenting the internal area,radiuses and wall thickness

Design data:

$\sigma_Y = 355$ MPa

$r_o = 254$ mm

$r_m = 247{,}75$ mm

$r_i = 241{,}5$ mm

$t = 12{,}5$ mm

$A_i = 1{,}83 \cdot 10^5$ mm^2

$\gamma_{M0} = 1{,}10$ (Norge, 2015)

By trial and error, the maximum internal pressure that the pipe can withstand is found to be 18,8 (N/mm^2). From the value of the internal pressure, the axial and the tangential stresses are determined:

Equation 4.2 gives:

$$\sigma_a = \frac{Pr_m}{2t} = \frac{18,8 \cdot 247,75}{2 \cdot 12,5} = 186,30 N/mm^2$$

Further the equation 4.3 gives the tangential stress:

$$\sigma_t = \frac{Pr_m}{t} = \frac{18,8 \cdot 247,75}{12,5} = 372,61 N/mm^2$$

The axial and the tangential stresses are in fact the principle stresses of the pipe, hence using the equation 4.6 the Mises stress is found:

$$\sigma_{VM} = \sqrt{\sigma_1^2 - \sigma_1\sigma_2 + \sigma_2^2} = \sqrt{186,30^2 - 186,30 \cdot 372,61 + 372,61^2} = 322,69 N/mm^2$$

According to the equation 4.4 the pipe yields when:

$$\sigma_{VM} \leq \frac{\sigma_Y}{\gamma_{M0}} = \frac{355}{1,10} = 322,72 N/mm^2$$

The value of Mises stress confirms the internal pressure the pipe can withstand. Now the shear stress between the ice plug and the wall pipe can be found. The shear stress can then again be compared with the adhesion and the ice's yield strength, as mentioned previously.

The force corresponding to an internal pressure of 18,8 (N/mm^2) can be found from the equation below:

$$F = P \cdot A_i = 18,8 \cdot 1,83 \cdot 10^5 = 3,44 \cdot 10^6 N$$

From the thermal analysis, a maximum ice plug at the top end was found to be approximately 0,5 (m). For a 0,5 (m) length, the area of the ice plug in contact with the pipe wall is:

$$A_{plug} = 2\pi r_i L_{plug} = 2 \cdot \pi \cdot 241,5 \cdot 500 = 7,59 \cdot 10^5 mm^2$$

Finally the shear force along the pipe wall is taken from the following equation:

$$\tau = \frac{F}{A_{plug}} = \frac{3,44 \cdot 10^6}{7,59 \cdot 10^5} = 4,54 N/mm^2$$

5.3.1.1 Examination of the strain rate

An approximation of the yield strength of ice can be evaluated from figure 4.3 if the strain rate in the ice plug due to water pressure is known. From the thermal analysis, it is possible to measure the amount of water that freezes per day. How fast the water freezes in the steel foundation is mainly influenced by the temperature. In figure 5.10 the frost depth inside the steel foundation is plotted for the conservative surface temperature given by Byggforsk (Byggforskserien, 2018).

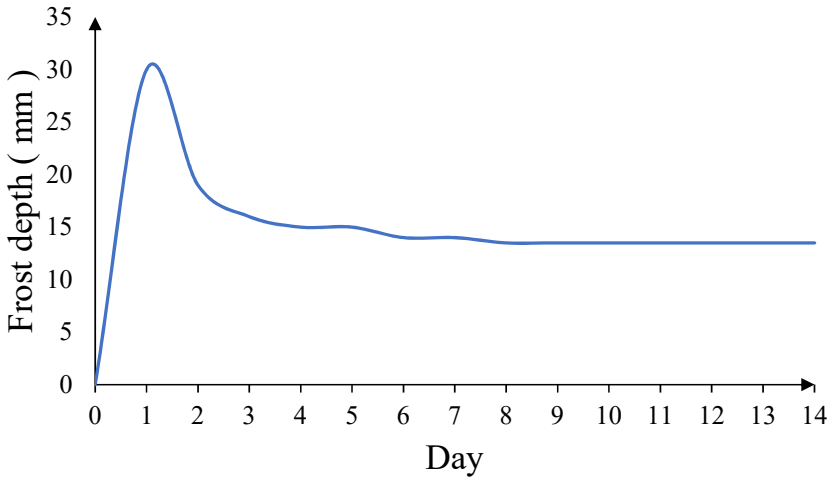

Figure 5.10: Frost depth per day

From the plot in figure 5.10, it can be seen that after one day of subzero temperatures, the frost depth is 30 mm, after which it starts to decrease. That is because the temperature takes more time to penetrate deeper. After 7 days, frost penetration becomes almost linear. This is not exactly correct; here, a more decline in frost depth was expected. For measuring the frost depth, the model was re-meshed with 10x10 (mm) elements that result in very high computation time, hence only a period of 14 days was simulated. Furthermore, even with an element size of 10x10 (mm), the analysis doesn't capture the very small changes in the frost depth. Therefore the linear section in the plot is present. However, the simulation gives an indication of the freezing depth per day. Further, in the calculations, the average conservative frost depth of 16 mm per day is chosen.

Based on the freezing depth per day the strain rate can be found, figure 5.11 illustrates the two plug scenario in question.

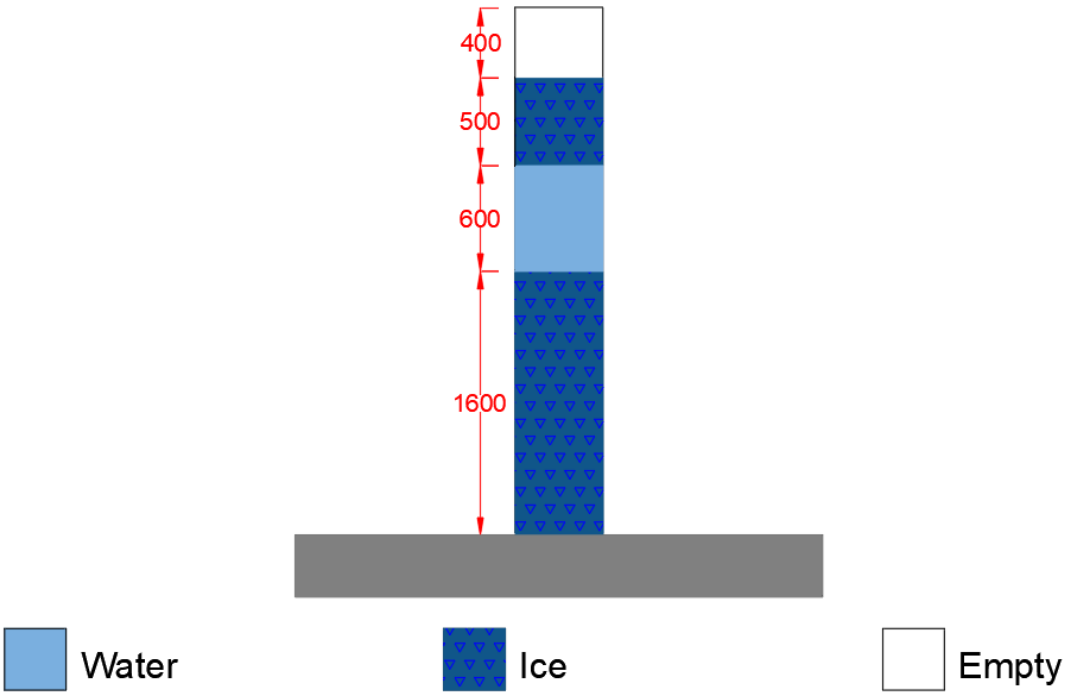

Figure 5.11: Illustration of the two plugs scenario (dimensions in mm)

The initial volume of the top ice plug is given by the following equation:

$$V_0 = \pi r^2 h_0 = \pi \cdot 241,50^2 \cdot 500 = 9,16 \cdot 10^7 mm^3$$

As mentioned previously when water freezes it expands by approximately 9,2% (Pople, 1987) and since per day 16 mm of it freezes, the change in volume per day is:

$$\Delta V = \pi \cdot 241,50^2 \cdot 16 \cdot 0,092 = 2,69 \cdot 10^5 mm^3$$

In the calculation above, it is assumed that the expansion of water is only in the vertical direction.

The strain increase per day is then given by:

$$\epsilon = \frac{\Delta V}{V_0} = \frac{2,69 \cdot 10^5}{9,16 \cdot 10^7} = 0,0029$$

Where the strain rate per second is:

$$\dot{\epsilon} = \frac{\epsilon}{time} = \frac{0,0029}{24 \cdot 3600} = 3,40 \cdot 10^{-8}/s$$

The strain rates for other surface temperature are calculated and given table 5.2:

Table 5.2: Strain rate at different temperatures

Temperature (°C)	Strain rate (1/s)
T= -5	$1,70 \cdot 10^{-8}$
T= Byggforsk	$3,40 \cdot 10^{-8}$
T= -20	$6,38 \cdot 10^{-8}$

From the diagram in figure 5.12 a strain rate of $3,40 \cdot 10^{-8}(1/s)$ gives the value of approximately 0,60 (N/mm^2) (magenta colour) for the yield strength of ice. It can be observed that the parameters are not very sensitive. For example an extreme freezing rate of 50 (mm) per day will give a strain rate of approximately 0,85 (N/mm^2) (green arrow).

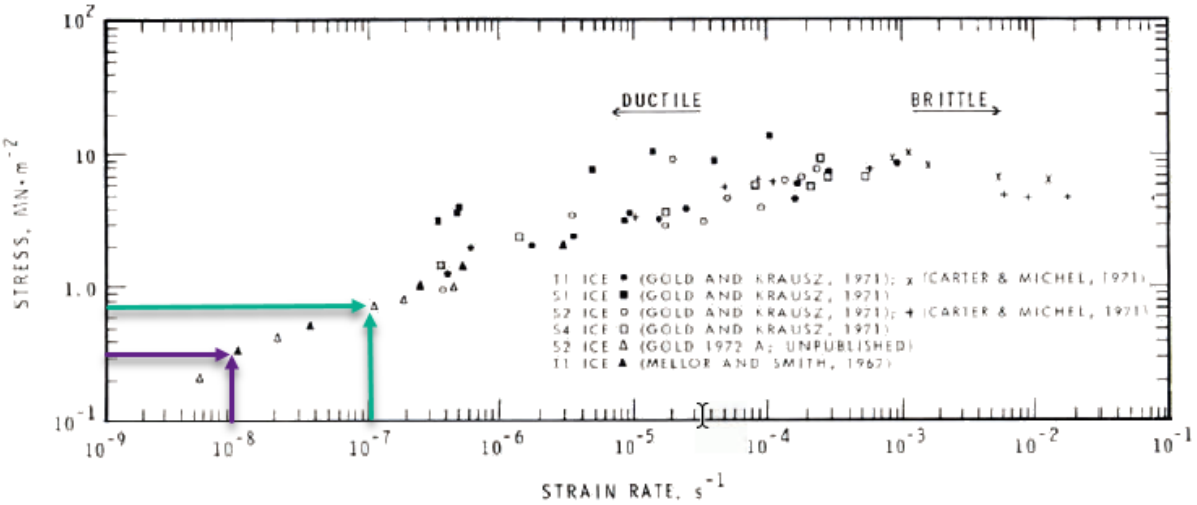

Figure 5.12: Yield strength of ice for different strain rates (Gold, 1977)

5.3.1.2 Results and discussion

The hollow section of the foundation can withstand a pressure build of 18,8 (N/mm^2). For this pressure, the shear stress along the wall pipe for an ice plug of 500 (mm) has found to be 4,54 (N/mm).

In theory chapter, according to (Gold, 1977), the ice has an adhesion strength of 0,5 (N/mm^2). Since the shear stress along the pipe wall is higher than the adhesion strength of ice means that the top ice plug will be pushed upwards. Therefore the pressure build will be released in the case when water is confined between two ice plugs.

Further, the yield strength of ice has been investigated. As described in the theory chapter, the yield strength of ice is dependent on a number of factors. Some of those factors are the strain rate, temperature, type of ice, direction of loading, purity of ice, etc. Because of the complexity of the factors, only an indication of the yield strength was found, hence conservative values were chosen. However, by finding the freezing rate per day from the thermal analysis, the yield strength of ice has been found to be approximately 0,60 (N/mm^2). For this value, the ice will start to yield before the shear stress capacity is exceeded.

Based on the findings the conclusion is clear, for these plug lengths, the pressure can not build up to burst the steel pipe, given that the adhesion and yield strength of ice is not significantly higher than what is used in the calculations.

5.3.2 Finite element analysis of two plugs scenario

The hand calculations from subsection 5.3.1 are in this section controlled with the finite element software Abaqus CAE by using a static, general simulation. The model has the same dimensions as the illustration in figure 5.11. Further, the bottom surface of the pipe is not allowed to move in the y-direction, and since the model is axis-symmetric, the center ax is pinned in the x-direction.The model is defined as one element and then partitioned in three parts, steel, top ice plug and bottom ice plug. Between the ice plugs the internal pressure found previously is applied. The Abaqus model is presented in figure 5.13 below.

5.3.2.1 Material properties

The materials used in the model are steel and ice, and their properties are given in table 5.3. Steel properties reflect the strength class of the pipe S355 structural steel. As explained previously, the properties of ice are dependent on many factors, the values used in this simulation are based on typical average values (Nimmo, 2004; Norge, 2015).

Table 5.3: Material properties

Element type	Material properties	
Steel	Young's modulus	210000 (N/mm^2)
	Poisson's ratio	0,3
Ice	Young's modulus	9000 (N/mm^2)
	Poisson's ratio	0,33

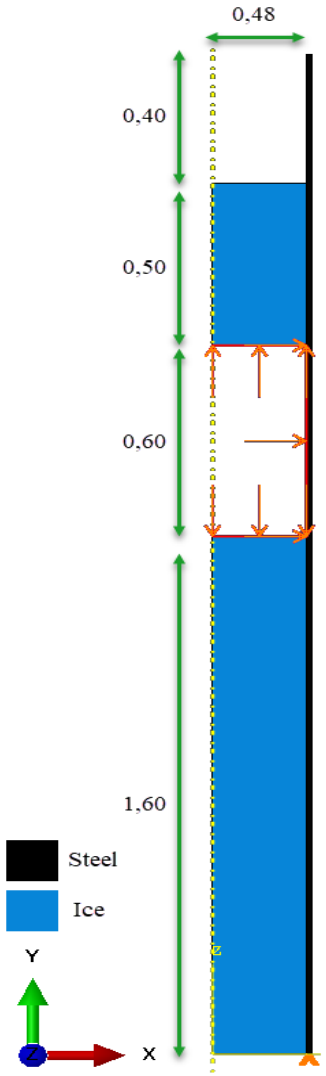

Figure 5.13: The geometry of the model for the two plugs scenario (dimensions in m)

5.3.2.2 Results and discussion

The distribution of Mises stress is given in figure 5.14. Because of the mesh density in order to be visible, the figure is divided into three parts. The figure to the left shows the distribution of stresses in the upper part of the model, followed by the middle part and

bottom part.

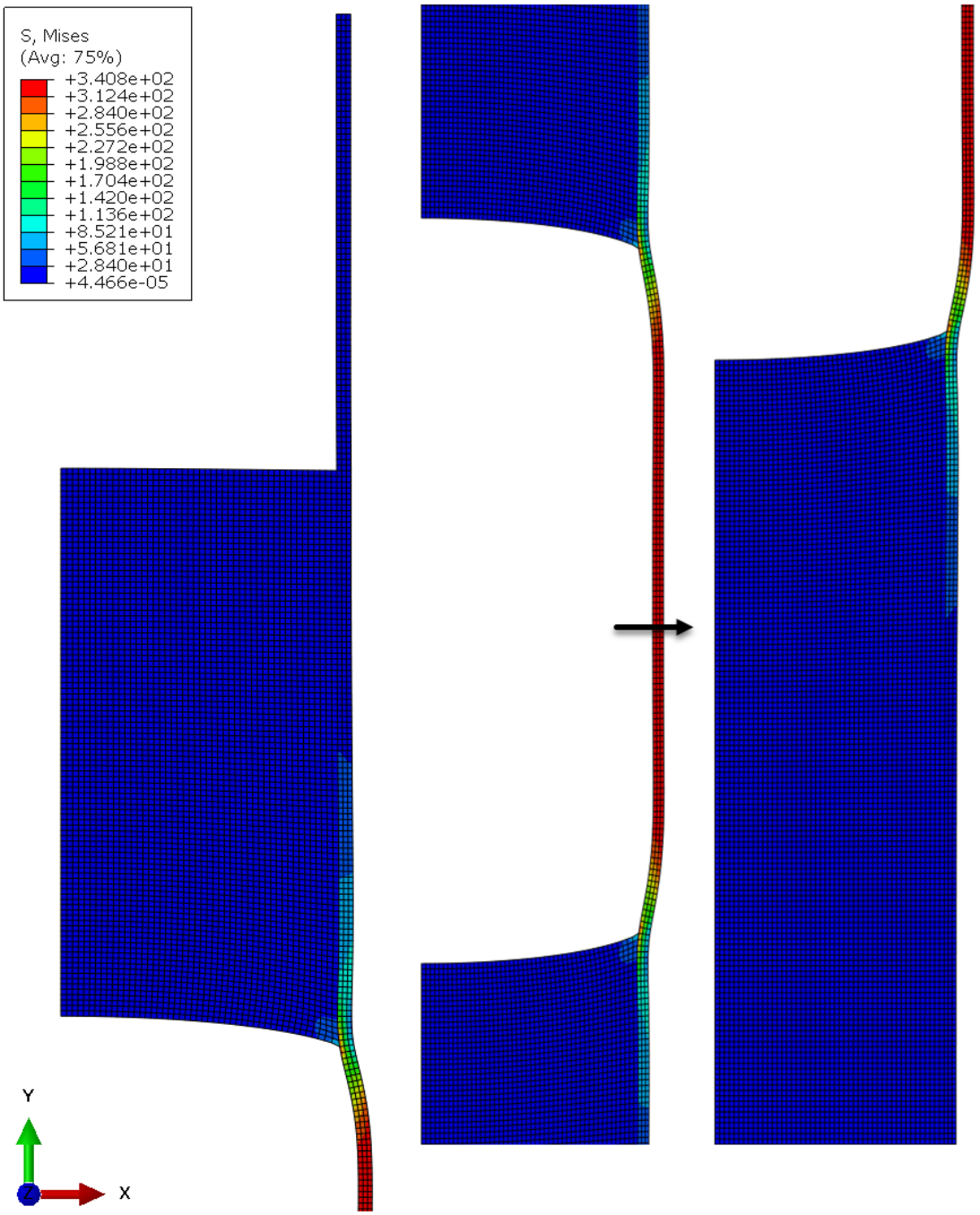

Figure 5.14: Stress contour in the model due to internal pressure (units N/mm^2)

As expected, the maximum stresses are on the pipe wall. Notice the 90°corners between the pipe and the plugs, if the whole model had been made from the same material with the same young's modulus, the highest stress concentrations would have been expected there. Since the ice is less stiff than the steel the stress concentration is not an issue in the corners. The stress plot from figure 5.15 is taken in the middle between the ice plugs ,

through the pipe wall. Location and the path direction is marked in figure 5.14 with a black arrow.

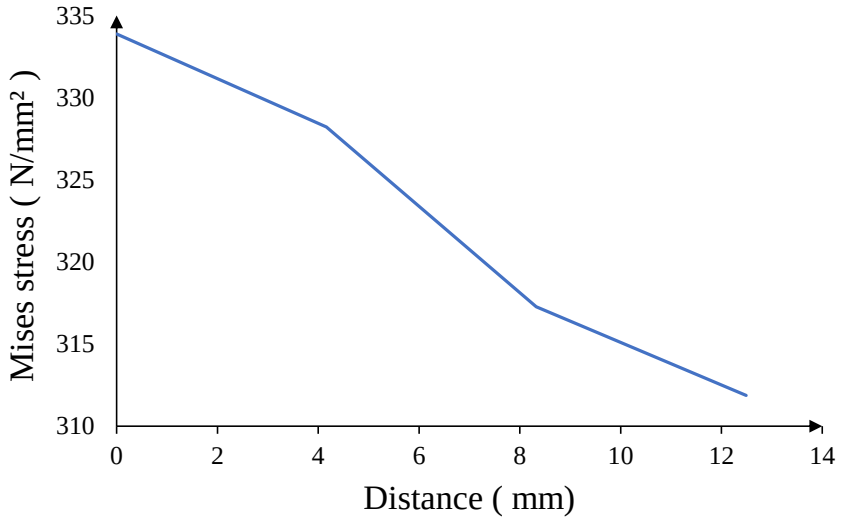

Figure 5.15: Stress distribution in the middle of the pipe

From figure 5.15, it can be seen that the stress distribution is not linear. This implies that bending stresses are present, which gives compression and tension stresses, and in addition, membrane stresses are present as well. The theoretical decomposition of stress into bending and membrane stresses is illustrated in figure 5.16 (Moss, 2004).

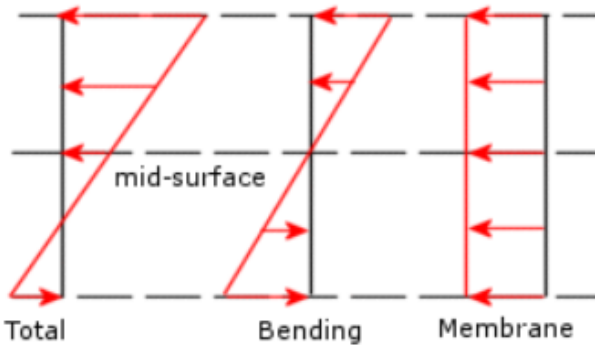

Figure 5.16: Decomposition of stress into a membrane stress and bending stress

Taking the average value from the total stresses plotted in figure 5.15 the membrane stress value of σ_m= 323,60 (N/mm^2) is obtained.

Further the shear stress between the top ice plug and the pipe wall is given in figure 5.17.

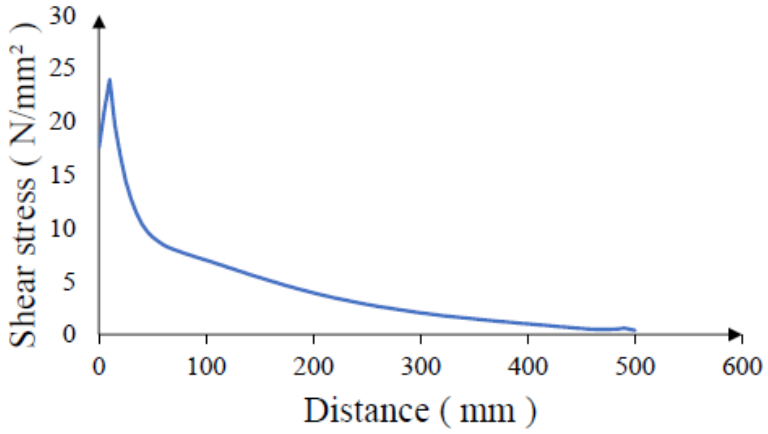

Figure 5.17: Shear stresses between the pipe wall and the top ice plug

The graph shows higher shear stress values closer to where the internal pressure is applied, towards the top surface, the stress is lower as expected.

It is important to mention that the plot was taken one element column from the pipe wall. Because of the bending that occurs in the pipe as a result, shear stresses are present as well.

Further, the shear stresses from the bending counteract the shear stress between the pipe wall and the ice plug.

By moving one element column from the contact region between the plug and the wall, a more accurate shear stress value is obtained. The average shear stress value found from the model is $\tau = 4{,}43$ (N/mm^2).

In table 5.4, the results from hand calculation and the finite element model are given. The percentage of error between the results is very small hence the calculations can be trusted and the main conclusion remains the same. Based on the calculations the pressure build between the plugs is not damaging for the pipe.

Table 5.4: Comparison of the results

Solution	Mises stress N/mm^2	Shear stress N/mm^2
Analytical	322,69	4,54
FE-model	323,60	4,43

6 Concluding remarks

The thesis aimed to investigate if the groundwater that can freely enter into the hollow section of the steel foundation can have a damaging impact on the structural integrity of the foundation when it freezes.

In order to know if the freezing of water is damaging for the steel foundation, first, the frost depth had to be found. The extent to which ice is formed was investigated by performing a set of thermal analyses. In total, three models were created in Abaqus CAE. The first two models were used to validate the analysis methodology for the third model. The third model simulated the frost depth of water inside the foundation. The results from the simulation gave a frost depth of a maximum of 2,4 m. Besides, the analysis showed that water could be trapped between two ice plugs. The formation of two ice plugs can be critical for the hollow section. A new thermal study was conducted to investigate the scenario of two ice plugs further. By assuming conservative input parameters, the simulation identified the formation of two fully formed plugs with water confined between them.

Further, a set of structural analyses was conducted to understand what the frost depth found from the thermal analysis meant to the structural integrity of the foundation. Based on the theory of ice, the formation of a single ice plug of 2,4 (m) was found not to be critical for the foundation.

In the second scenario, the thermal expansion of ice was investigated. When an ice plug is fully formed, if the temperature keeps decreasing, the ice begins to shrink. Further, when the temperature rises again, the ice will start to expand, creating pressure if the expansion is restricted, as in the case of the steel foundation. The pressure created by the expansion of ice was simulated in Abaqus CAE, and the result showed that the strength capacity of the pipe was significantly higher than the force applied by the ice.

For the third and last scenario where two ice plugs with water trapped between them are formed, hand calculations and an FE-model were performed. The steel pipe capacity was investigated, and it has been found to be higher than the adhesion and the yield strength of ice. Both the hand calculations and the finite element analysis converged well, leading to the following conclusion: the formation of two ice plugs does not affect the

structural integrity of the foundation given that the adhesion and yield strength of ice is not significantly higher than what was used in the calculations. Furthermore, there will likely be snow at least parts of the winter season. The snow on the ground acts as an insulation, slowing the frost penetration into the ground and into the foundation. Meaning the size of the ice plug/plugs is reduced. Because of the complexity and the uncertainty of the parameters, the thesis was based on evaluating worst-case scenarios. The structural integrity of the foundations is critical for the stability of the lattice steel towers. And furthermore, the stability of the towers is crucial for the supply of electricity, hence this thesis approach.

References

Akyurt, M., Zaki, G., and Habeebullah, B. (2002). Freezing phenomena in ice–water systems. *Energy conversion and management*, 43(14):1773–1789.

Alavala, C. R. (2008). *Finite element methods: Basic concepts and applications*. PHI Learning Pvt. Ltd.

Bai, Y. and Bai, Q. (2010). Chapter 14 - heat transfer and thermal insulation. In Bai, Y. and Bai, Q., editors, *Subsea Engineering Handbook*, pages 401 – 450. Gulf Professional Publishing, Boston.

Byggforskserien, B. . (2018). Klimadata for termisk dimensjonering og frostsikring.

Cengel, Y. (2014). *Heat and mass transfer: fundamentals and applications*. McGraw-Hill Higher Education.

Fransson, L. (1988). *Thermal ice pressure on structures in ice covers*. PhD thesis, Luleå tekniska universitet.

French, H. M. (2017). *The periglacial environment*. John Wiley & Sons.

Gold, L. W. (1977). Engineering properties of fresh-water ice. *Journal of Glaciology*, 19(81):197–212.

Gordon, J. R. (1996). An investigation into freezing and bursting water pipes in residential construction. Technical report, Building Research Council. School of Architecture. College of Fine and ....

Hibbitt, Karlsson, and Sorensen (1997). *ABAQUS: theory manual*. Hibbitt, Karlsson & Sorensen.

Ibrahim, A., Ryu, Y., Saidpour, M., et al. (2015). Stress analysis of thin-walled pressure vessels. *Modern Mechanical Engineering*, 5(01):1.

institutt, M. (2020). eklima.

Irgens, F. (2006). *Fasthetslære: Fridtjov Irgens*. Tapir akademisk.

ISO, S. (2001). 13793: 2001. *Thermal performance of buildings. Thermal design of foundations to avoid frost heave*.

John, H., Lienhard, I., and Lienhard, V. (2006). A heat transfer textbook.

Makkonen, L. (2012). Ice adhesion—theory, measurements and countermeasures. *Journal of Adhesion Science and Technology*, 26(4-5):413–445.

Marchenko, A., Lishman, B., Wrangborg, D., and Thiel, T. (2016). Thermal expansion measurements in fresh and saline ice using fiber optic strain gauges and multipoint temperature sensors based on bragg gratings. *Journal of Sensors*, 2016.

Melinder, Å. (2007). *Thermophysical properties of aqueous solutions used as secondary working fluids*. PhD thesis, KTH.

Mellor, M. (1977). Engineering properties of snow. *Journal of Glaciology*, 19(81):15–66.

Moss, D. R. (2004). *Pressure vessel design manual*. Elsevier.

Nimmo, F. (2004). What is the young's modulus of ice? In *Workshop on Europa's Icy Shell: Past, Present, and Future*.

Norge, S. (2015). Ns-en 1993-1-1: 2005+ a1: 2014+ na: 2015. *Standard Norge*.

Pople, S. (1987). *Explaining physics*. Open University Press.

Ramires, M. L., Nieto de Castro, C. A., Nagasaka, Y., Nagashima, A., Assael, M. J., and Wakeham, W. A. (1995). Standard reference data for the thermal conductivity of water. *Journal of Physical and Chemical Reference Data*, 24(3):1377–1381.

Randhawa, K. S. (2018). *The measurement of the Young's modulus of ice with ultrasonic waves*. PhD thesis, Technische Universität Hamburg.

Schulson, E. M. (1999). The structure and mechanical behavior of ice. *Jom*, 51(2):21–27.

TC88-MT, I. (2005). Iec 61400-3: Wind turbines–part 1: Design requirements. *International Electrotechnical Commission, Geneva*, 64.

Appendix

A1 Calculation of the temperature throughout the soil

Table A1.1: Temperature throughout the soil from the linear soil analysis

Depth (m)	Temperature Abaqus (°C)	Temperature analytical solution (°C)
0,00	20,000	20,000
0,05	19,236	19,211
0,10	18,472	18,424
0,15	17,708	17,640
0,20	16,944	16,863
0,25	16,180	16,093
0,30	15,416	15,332
0,35	14,652	14,583
0,40	13,888	13,846
0,45	13,124	13,123
0,50	12,360	12,417
0,55	11,769	11,727
0,60	11,179	11,055
0,65	10,589	10,403
0,70	9,998	9,772
0,75	9,408	9,161
0,80	8,818	8,573
0,85	8,228	8,007
0,90	7,637	7,465
0,95	7,047	6,945
1,00	6,457	6,450
1,05	6,097	5,978
1,10	5,738	5,529
1,15	5,378	5,104

Table A1.1 continued from previous page

Depth (m)	Temperature Abaqus (°C)	Temperature analytical solution (°C)
1,20	5,018	4,703
1,25	4,659	4,324
1,30	4,299	3,968
1,35	3,940	3,633
1,40	3,580	3,320
1,45	3,221	3,028
1,50	2,861	2,756
1,55	2,684	2,503
1,60	2,506	2,269
1,65	2,329	2,052
1,70	2,151	1,852
1,75	1,974	1,668
1,80	1,796	1,499
1,85	1,619	1,344
1,90	1,441	1,203
1,95	1,264	1,074
2,00	1,086	0,957
2,05	1,014	0,851
2,10	0,941	0,755
2,15	0,868	0,668
2,20	0,795	0,590
2,25	0,722	0,520
2,30	0,649	0,457
2,35	0,577	0,401
2,40	0,504	0,351
2,45	0,431	0,307
2,50	0,358	0,268
2,55	0,333	0,233
2,60	0,307	0,202

Table A1.1 continued from previous page

Depth (m)	Temperature Abaqus (°C)	Temperature analytical solution (°C)
2,65	0,282	0,175
2,70	0,256	0,151
2,75	0,231	0,130
2,80	0,205	0,112
2,85	0,180	0,096
2,90	0,155	0,082
2,95	0,129	0,070
3,00	0,104	0,060
3,05	0,096	0,051
3,10	0,088	0,043
3,15	0,081	0,037
3,20	0,073	0,031
3,25	0,065	0,026
3,30	0,058	0,022
3,35	0,050	0,018
3,40	0,042	0,015
3,45	0,034	0,013
3,50	0,027	0,011